








Metal-Organic Framework Nanosheets (MONs): A Review On Interfacial Syntheses And Applications Of Coordination Nanosheets

Suzaliza Mustafar ^{1,*}, Anis Kharul Nada Mohd Yusuf ¹, Leah Ma. Borines ², ETTY Nurlia Kusumawati ³, Azlan Kamari ¹, Noorshida Mohd Ali ¹, Yusnita Juahir ¹

¹ Department of Chemistry, Faculty of Science and Mathematics, Universiti Pendidikan Sultan Idris, 35900 Tanjong Malim, Perak, Malaysia; suzaliza@fsmt.upsi.edu.my (S.M.); aniskharulnada@gmail.com (A.K.N.M.Y.); azlan.kamari@fsmt.upsi.edu.my (A.K.); noorshida@fsmt.upsi.edu.my (N.M.A.); yusnita@fsmt.upsi.edu.my (Y.);

² Department of Chemistry, University of Connecticut, 55 North Eagleville Road, Unit 3060, Storrs, Connecticut, U.S.A.; ma_leah.borines@uconn.edu (L.M.B.);

³ Chemistry Course, Faculty of Science and Engineering, Iwate University, 4-3-5, Morioka, 020-8551, Japan; etty01@iwate-uc.ac.jp (E.N.K.);

* Correspondence: suzaliza@fsmt.upsi.edu.my (S.M.);

Scopus Author ID 56607376300

Received: 17.12.2021; Accepted: 12.01.2022; Published: 12.02.2022

Abstract: Two-dimensional (2D) nanomaterials such as metal-organic nanosheets (MONs) are exceptionally fascinating for electronics, photonics, optoelectronics, spintronics, and magnetism due to their enticing properties such as tuneable structures of ligands and metal complexes, intensify porosity and conductivity as well as successful facile fabrication of larger domains of the 2D materials. Owing to their unique qualities, such as intrinsic electronics and optical attributes, 2D materials have achieved tremendous breakthroughs in the direct applications of MONs. Based on recent research findings, MONs have been regarded as promising materials for surface functioning. At the same time, the intrinsic band structure and electronic properties may be rationally regulated via structural change, which can be the focal point of advanced materials design, processing, and progress. In this context, the potential to utilize different ligands and a vast number of coordinative atoms become important in designing 2D materials to address the tremendous needs of industry players. This review focuses on coordination nanosheets, which is a type of molecule-based nanosheets. The examples of coordination nanosheets are discussed in Section 1. In Section 2, surveys research on bottom-up coordination nanosheets synthesized through the liquid/liquid and gas/liquid interfacial reactions are discussed. Section 3 discusses the potential applications of coordination nanosheets in nanomaterial science. Overall, this review provides a useful source of information for researchers working on advancing 2D nanomaterials, particularly coordination nanosheets.

Keywords: two-dimensional; metal-organic nanosheets; coordination nanosheets

© 2022 by the authors. This article is an open-access article distributed under the terms and conditions of the Creative Commons Attribution (CC BY) license (<https://creativecommons.org/licenses/by/4.0/>).

1. Introduction

Metal-organic frameworks (MOFs) are three-dimensional (3D) crystalline materials in general, although it is being incorporated with laminar 2D nanosheet motifs to produce 3D crystals [1]. To form supramolecular frameworks, MOFs typically require a number of strong and reversible organic–metal bonds [2]. The most prominent form factor of metalorganic material is 2D MONs. MOFs nanosheets [3], metal-organic surfaces (MOSs) [4], metal-organic

layers (MOLs) [5], metal-organic flakes [6], metal-organic graphene analogs (MOGs) [7,8], organometallic sheets [9], two-dimensional MOFs [10], coordination nanosheets [10], two-dimensional coordination polymers [11], single-layered MOFs based materials (MOFenes) [12] and hybrid organic-inorganic [13] nanosheets have all been used to describe MONs.

Even though there are significant differences between some of the terminologies used in these descriptions, they are grouped under a common name to highlight the similarities in the fundamental chemistry, synthesis method, characterization techniques, and attribution. In this context, a broader term was used in this review, including materials that exhibit 'nanosheet'-like structure and its characteristics.

MONs are made of coordination between ligands and metal ions or clusters having 2D continuous connectivity but merely non-covalent engagements in a 3D form. Moreover, MONs must be in the form of free-standing sheets or as layers in a bulk material that is detachable from a surface or other scaffolds. The primary idea in constructing 2D nanosheets is to create materials that have weak interactions across the layers in the bulk material but retain robust directional interactions within a plane. One of the examples is Graphene which possesses covalently bonded carbon-carbon atoms forming a hexagonal lattice, the layers of which are bound together by comparatively moderate dispersion interactions [14]. Interestingly, within-layer connectivity of MONs can be established via coordination between organic ligands and metal ions or inorganic clusters, or a combination of the two [15]. Any 3D connection is usually a combination of ionic interactions, hydrogen bonding, or dispersion, which allows for the separation and isolation of particular layers. Due to their intriguing physics, 2D materials have been of interest in the last two decades, of which the most prominent is graphene [16,17]. Nevertheless, due to its zero bandgap, graphene is unfit to be employed in semiconductor-based devices [18]. This constraint opens the door to a wide range of studies into the development of alternative 2D-layered structures [19–27], such as transition metal chalcogenides [28], hydroxides [29], carbides [30], graphdiynes [31], boron nitride [32], black phosphorus nanosheets [33] and MXenes [34]. Other compounds namely Germanene [35] compound from the graphene family is also used for the application in electronics [36], photonics [37], optoelectronics [38], spintronics [39], magnetism [40] and others [41]. To enhance the physical properties of the 2D materials, materials science research was conducted to functionalize and flexibly adjust the electronic band structure of these materials [18,42,43].

Coordination nanosheets, the family of MONs, display interesting characteristics and functional groups that enable chemical functionalization and subsequently aid in developing molecular superstructures. Metal complex motifs have unique magnetic, redox, and photo properties that may be used to express desired functions in coordination nanosheets. The most obvious feature of coordination nanosheets is their wide range of diversity and the unlimited combinations of metal atoms or ions and organic molecules that could be used to fabricate molecule-based nanosheets [44,45]. Even though molecule-based nanosheets are more diversified than inorganic nanosheets, their synthesis and characterization have proved to be challenging hence impeding commercialization. Although molecule-based nanosheets have been considered theoretically for many years [46], they did not become a reality until the early 2000s.

This is a review of the coordination nanosheets, which is a type of molecule-based nanosheet. Metal ions/atoms/clusters and organic ligand molecules make up a coordination nanosheet, whereas the coordination bonds between them create a 2D polymeric framework. This review starts with a discussion on several examples of nanosheets before introducing the

typical synthetic strategies for interfacial synthesis. Finally, the applications of coordination nanosheets are summarized.

1.1. Examples of coordination nanosheets.

Varaksa, Magnera, and Michl reported the first example of a coordination nanosheet on a Hg surface [47] using 1,3,5-tris[10-(3-ethylthiopropyl) dimethylsilyl-1,10-dicarbocloso-decaboran-1-yl]benzene as the starting material in a Langmuir-Blodgett (LB) fitted with a potentiostat. Even though the 2D coordination network structure was not observed, the hypothesized hexagonal network bound by Hg ions was shown with Austin Model 1(AM1)-optimized structure. The bridging links between the sulfide molecules were S–Hg²⁺–S or S–Hg₂²⁺–S and the hexagon motif with a length of 1.89 nm, which is similar to the predicted Langmuir isotherm. According to the author, the difference between the observed and calculated values may be due to the misrepresentation of the hexagon's relative size related to defects and grain boundaries. Although there is no further characterization and isolation of discrete structures of the nanosheets, this work paved the way for the development of coordination nanosheets.

1.1.1. Carboxylate-based coordination nanosheets.

The most often used organic ligand for fabricating coordination nanosheets is polycarboxylates, which are well-liked for their stable, directed coordination chemistry and a broad range of commercially available ligands. Isostructural coordination nanosheets have been shaped employing an assortment of metal ions (Cu, Zn, Co), longer direct diacid chains [48], 1,3- benzene dicarboxylate derivatives [49,50], and 1,4-benzene dicarboxylate [51–53]. Cao *et al.* established an infinite 3,6-connected 2D network with a kagome dual (kgd) topology by integrating 3-connected carboxylate ligands, originally benzene-1,3,5-tribenzoate (BTB) moieties, with the Hf⁴⁺ cluster [Hf₆(μ₃₋₀)₄(μ₃₋₀H₄ (carboxylate)₁₂] [5]. Coordination nanosheets based on the tetrakis (4-carboxyphenyl)porphyrin (TCPP) structure have been synthesized using a variety of metal paddlewheels [54–56]. The paddlewheel motif comprises four carboxylate ligands arranged in a plane around two metal cations capped with axial ligands, is an excellent secondary building block to generate coordination nanosheets. This motif also facilitates the fabrication of bimetallic coordination nanosheets by coordinating numerous metal ions at the paddlewheel and porphyrin units [57].

1.1.2. N-donor-based coordination nanosheets.

4,4-bipyridine (bpy), a neutral N-donor system, was utilized to construct a layered framework of Cu(bpyh(OTf)₂) while the trifluoromethanesulfonate (OTf) counterions bound weakly at the interacting layers [58]. Transmission electron microscopy (TEM) and atomic force microscopy (AFM) revealed the single and few layers of nanosheets with crumpling and rolling to create nanoscrolls. This thus emphasizes the system's flexibility. Several different tri- and hexadentate terpyridine (tpy) building blocks have also been utilized to self-assemble monolayers at interfaces through coordination to various metal ions [59–63]. These multidentate building units offer strong coordinating interactions with a high degree of connectivity through their multidentate binding. The single-layered nanosheets produced via interfacial assembly are mechanically robust and may have lateral dimensions up to several cm. However, the degree of crystallinity is probably low [64]. A structurally similar family of

coordination nanosheets has also been fabricated by using coordination between tri- or tetra-dipyridyl ligands and tetrahedral zinc ions [65,66].

1.1.3. Diamine/dithiolene-based coordination nanosheets.

A series of coordination nanosheets, which were constructed between aromatic bis(dithiolenes) and square-planar metal ions, have garnered a great deal of attention due to their remarkable electrical properties. For example, the reaction between benzenehexathiol (BHT) and d^8 metal ions such as Ni(II) [67] and Pd(II) [68,69] created six-fold symmetry planar nanosheets with the Ni(II) bis(dithiolene) motif. These complexes show a significant charge delocalization across the three metalladithiolene units in mixed-valent states through the phenylene linker. Triphenylene hexathiolate with nickel [70] and cobalt [71] have been used to synthesize expanded variants of these systems besides the amino analogs. In acetylacetonate, the interfacial reaction between hexaminobenzene and metal ions such as Ni^{2+} , Cu^{2+} , and Co^{2+} resulted in several microns wide of slightly conducting thin sheets. Although individual sheets of these materials have not been separated, expanded counterparts of these layered materials have been produced to establish semi-conducting frameworks by reacting hexaminotriphenylene with Ni and Cu ions [72–74]. Mixed amine/thiolene coordination nanosheets with similar structures have also been synthesized by combining triphenylene hexathiolate and hexaminotriphenylene with Ni^{2+} or Co^{2+} ions [75].

2. Interfacial Synthesis of Coordination Nanosheets

There are two different approaches to the synthesis of coordination nanosheets, which are known as "bottom-up" and "top-down". In the "bottom-up" method, the nanosheets are fabricated directly as discrete entities through numerous approaches to induce the crystallization process. While for the "top-down" method, the nanosheets are dissociated from the bulk layered materials such as graphene sheets by mechanical isolation from graphite. However, the coordination bonding between the layers of coordination nanosheets is more versatile than in graphene or other inorganic materials. Therefore, this paves the way for fabricating coordination nanosheets from solution and alleviates some of the difficulties related to irreversible bond formation. This also implies that gentler treatments may be needed, and the structures may be rearranged. The "bottom-up" method will be discussed, specifically the interfacial synthesis. In interfacial synthesis, the use of phase interfaces such as air-liquid [61,66,76–82] or liquid-liquid [65,83–86] is the alternate technique for steering the crystal development into two dimensions. These techniques operate in ambient circumstances in general. Langmuir-Blodgett troughs have been used to show liquid-gas interfacial growth in which a ligand solution in a volatile organic solvent is placed on top of an aqueous phase of metal ions [81,82,87]. Surface compression may induce huge extended nanosheets with sub-mm scale domains with an unknown crystallinity of the vast sheets. Furthermore, films may also be constructed using layer-by-layer deposition of these larger nanosheets. Nishihara and the team have reported more comprehensive techniques, and several nanosheets were generated using these methods [88,89]. The interface-assisted techniques were often applied in the initial stages of the bottom-up methods by assembling the organic ligands and metal ions at different interfaces [90]. The area of the reaction interface hugely affects the size of the nanosheets. Creating an interface with a significant reaction area and appropriate metal ions-ligand molecular diffusion ability is the key to constructing extended nanosheets [91]. The interfacial

synthesis may be conducted at room temperature without a controlled environment. Generally, the interfacial synthesis is divided into two groups based on the interface position, whether liquid/liquid interface or gas/liquid interface synthesis.

2.1. Liquid/liquid interfacial synthesis.

The coordination interaction between metal ions in an aqueous solution and organic ligands in organic solvents produces coordination nanosheets at the interfacial of two immiscible solvents. This technique has been used to fabricate a number of multilayers and ultrathin coordination nanosheets, either none-conjugated or π -conjugated nanosheets. Bis(dipyrrinato)zinc(II) complex is the example of a none-conjugated nanosheet that was synthesized at the H₂O/dichloromethane (CH₂Cl₂) interface where the top layer is zinc(II) aqueous acetate solution. In contrast, the bottom layer is the three-way dipyrin ligand (L1) in CH₂Cl₂ [66]. An orange transparent film (N1) was observed at the H₂O/CH₂Cl₂ interfacial region with 700 nm thickness, equivalent to 580 layers of single-layer N1. The liquid/liquid interface technique may also be used to synthesize non-conjugated nanosheets based on non-coplanar organic linkers such as dipyrin and terpyridine. The coordination process between Fe²⁺ ions and terpyridine ligand [86] yielded 180-nm-thick bis(terpyridine)Fe(II) complex π -conjugated nanosheets at the CH₂Cl₂/H₂O interface. The coordination interaction between transition metal ions and planar organic ligands at the liquid/liquid interface may produce ultrathin π -conjugated nanosheets with hexagonal layered architectures such as metal bis(dithiolene) complexes [71,83,92,93], metal hexaaminobenzene [94], bis(aminothiolato)nickel [69] and cobalt dithiolene framework [95]. For example, multi-layered bis(iminothiolato)nickel π -conjugated coordination nanosheets with a size of over 10 μ m were synthesized at the liquid/liquid interface via a coordination interaction between 1,3,5-triaminobenzene-2,4,6-trithiol aqueous solution and bis(2,4-pentanedionato)nickel(II) (Ni(acac)₂) in CH₂Cl₂ resulting in a semiconducting nanosheet [75]. In liquid/liquid interfacial synthesis, an aqueous solution of the metal ions is gently placed on top of the organic ligand solution to create a liquid/liquid interface, as shown in Figure 1.

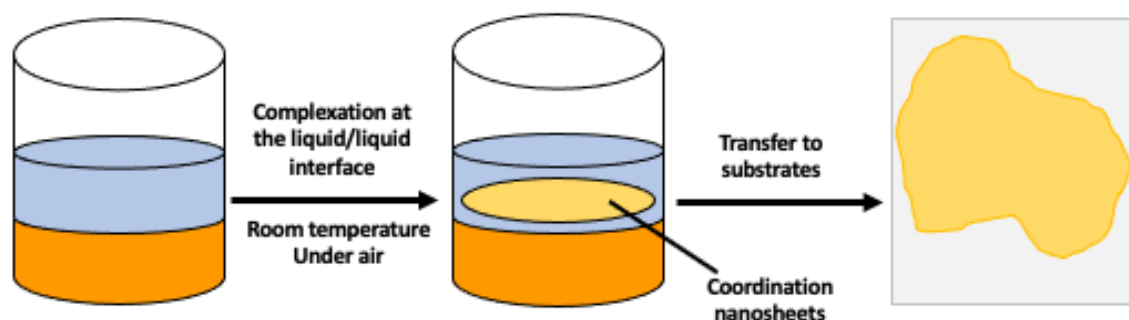
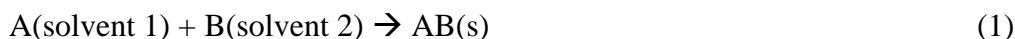


Figure 1. Schematic diagram of the liquid/liquid interfacial synthesis.

The solution was gently removed once the nanosheet had formed. If the organic solvent has a lower density than water, it will rise to the top of the layering system. Although the domain size may reach 10 cm, there is space for debate regarding the quality and crystallinity of the coordination nanosheets generated using this method. Sakamoto *et al.* reported a novel bis(dipyrrinato)zinc(II) complex (N2) micro- and nanosheets, which was formed by the coordination between zinc ions and a 4-fold symmetry porphyrin–dipyrrin hybrid ligand [66]. The N2 was then utilized as the active material in a photoelectric conversion system by leveraging the existence of porphyrin and bis(dipyrrinato)zinc(II) complex units that has a wide

range of visible-light spectrum absorption bands [65]. The coordination process at the liquid/liquid interface often results in multilayer nanosheets. Some modifications to the method may produce single-layer nanosheets. The formation of ultrathin nanosheets can be induced by controlling horizontal and vertical growth [96–102].

An in-situ interfacial chemical reaction occurs at the liquid/liquid interface, resulting in nanosheets obtained at the liquid/liquid contact. The case of a generic reaction is represented by (1), as shown in Figure 1.



The groundbreaking study by Amellot *et al.*, who produced thin films using a water/1-octanol biphasic solution, has synthesized several MOFs structures in-situ at liquid/liquid interfaces using many methods [103]. By using a biphasic water/chloroform system, thin films were formed on the inner or outer side of the polymeric hollow fiber membranes resulting in membranes with excellent performance in gas separation operations [104]. Joshi *et al.* synthesized various organometallic polymers of catechol–metal by in-situ reaction of a catechol derivative in toluene or dichloromethane with Fe²⁺ or Cu²⁺ precursors in an aqueous solution. Testing for oil/water combinations demonstrated superhydrophobic films with excellent separation efficiency [105]. The liquid-liquid interface synthesis technique is not only restricted to immiscible solvents but may also be used in organic solvents with a variety of densities. A novel method for the fabrication of free-standing thin films based on miscible liquid/liquid interfaces (MLLI) at room temperature has been developed by Bai *et al.* In order to prepare the nanosheets, a solution of Cu²⁺ ions in N,N-dimethylformamide/acetonitrile (DMF/ACN) was sprayed onto the surface of a DMF/ACN solution containing the ligand. This resulted in a freestanding film at the liquid interface [106]. In addition, coordination nanosheet capsules made of 2D coordination polymers were successfully synthesized by using a spherical liquid/liquid interface of DCM droplets in water [107]. For the first time, an electrochromic (EC) hyperbranched coordination nanosheet containing an iron(II) ion and a three-arm terpyridine (3tpy)-based ligand has been created on a liquid-liquid interface [108]. From the microscopic examination of the coordination nanosheets film deposited on ITO, the formation of a homogenous nanosheet layer with 350 nm thickness was observed. Upon switching on the fabricated solid-state electrochemical device (ECD), it undergoes a reversible redox reaction (Fe²⁺ to Fe³⁺) accompanied by a color change over several cycles. Besides fabricating the metal-oxide framework nanosheets, the liquid-liquid interface synthesis method can fabricate covalent framework nanosheets via polymerization of organic molecules at the interface of two-layered solvents [109–112]. The production of covalent framework nanosheets is highly dependent on the order of the added solvents. Dey *et al.* mentioned that an interfacial crystallization approach might be used to fabricate ultra-thin covalent framework nanosheets with 50 to 90 nm thicknesses [113].

2.2. Liquid/liquid interfacial route (LLIR).

Some of the most significant accomplishments of a new method known as the Liquid/Liquid Interfacial Route (LLIR) is the ability to synthesize various types of materials as thin films and deposit the thin films as single- or multi-component materials over any substrate, including flexible substrates. Moreover, the deposited thin films' thickness, homogeneity, and transparency can be controlled. The well-known deposition techniques such as chemical vapor deposition (CVD) have some disadvantages whereby numerous novel and complex materials are unable to be deposited due to insolubility, infusibility, and dispersibility

of the material. Methods requiring high temperatures are not suitable for polymers deposition onto plastisol. Therefore, LLIR is particularly intriguing because it enables the in-situ synthesis of multi-component materials directly as thin films stabilized at the liquid/liquid interface. This could solve the issues relating to the preparation and processing in a single pot and single-step procedure [114].

In LLIR, two immiscible liquids are brought into contact with one another. In the first option, the solid deposited as a thin film has been previously dispersed in one of the liquids. Then, the L/L system is stirred or placed in an ultrasonic bath to produce droplets of one liquid phase spread across the other liquid phase, similar to a macro-emulsion. After some time, the stirring is stopped, and spontaneous self-organization of the scattered solid at the interface between the two liquids is seen. This results in a linked film resembling a flexible skin. Once the material has been stabilized as a film at the interface, it can be easily removed and deposited over suitable substrates by immersing the substrate in a bottom-phase liquid below the film and lifting the substrate in the film direction in a controlled manner. The most important alternative in LLIR is a hybrid of the two preceding processes, a chemical reaction in the presence of one or two dispersed materials and a hybrid of the two preceding techniques. The resulting solid, a thin film at the liquid/liquid contact, will be a nanocomposite between the previously dispersed solid and the solid formed by the chemical reaction. The particle size, shape, chemical composition, surface composition, and roughness are important in this process. The transfer process from the liquid/liquid interface to the solid substrate directly affects the quality of the deposited film. It is possible to utilize a variety of various sizes and shapes of substrates.

Additionally, deposition may be performed on both sides of the substrate by drawing the substrate perpendicular to the liquid/liquid film. Multiple successive depositions in a layer-by-layer method over the same substrate are also possible. The thickness of the film has an impact on both transparency and conductivity. Therefore, achieving consistent control over the thickness and homogeneity of the thin films is one of the most important aspects to be considered in any synthesis method. One of the most intriguing aspects of the LLIR is that these parameters may be adjusted by simply controlling the quantity of the material prior to the deposition process. Another method of controlling the film thickness is changing the reaction flask's size or changing the temperature. The planar interfacial area between the two immiscible liquids will increase by approximately a factor of two. In this approach, the dispersed solid is evenly distributed across the liquid/liquid contact resulting in the thinnest layer interface [115]. The LLIR has shown exceptional efficiency in synthesizing thin films of organic, inorganic, or metallorganic bidimensional films such as COFs, TMDs, metal-organic frameworks, or metalloporphyrins. LLIR is able to produce thin films with a number of distinct attributes compared to the conventional deposition routes. For example, the deposited film could originate from existing material or be synthesized in-situ using the one-pot method. This simple, inexpensive procedure does not require expensive or complex equipment and can be carried out in an uncontrolled environment. In contrast to other techniques, the LLIR does not require high temperatures. Thus, some techniques can avoid substrate restrictions in which deposition over plastic substrates is not possible. In the era of cutting-edge technology requiring flexibility, conductivity, and transparency such as flexible organic solar cells, stretchable sensors, flexible and transparent electrodes, LLIR is suitable to be engaged in industrial-scale production. Although the roll-to-roll continuous deposition method was the first large-scale thin-film manufacturing [116], researchers may create many alternative ways in the near future.

2.3. Gas/liquid interfacial synthesis.

The LB thin film has been studied extensively since Langmuir and Katherine Blodgett first discovered it. The researcher found that the organic layer was evenly formed on a solid substrate by inserting the solid substrate vertically into the water subphase. The term "Langmuir film" refers to a monolayer that floats on the liquid surface, while the "LB film" term refers to a multi-layered film [117,118]. Fabrication of relatively few- or single-layer thick coordination nanosheets in a short time is possible by conducting the synthesis in a Langmuir–Blodgett (LB) trough. When the organic solvent evaporates, a coordination nanosheet is formed dispersedly at the gas/liquid interface. In order to collect the pieces, the surface area in the LB trough must be reduced to increase the density per unit area. The domain size may reach a sub-millimeter scale. Benzene [67,92,119], carboxyl [82,87,120], terpyridine [61,77] and cyanide groups [121,122] have all been used to fabricate coordination nanosheets. Following the discovery of the LB method, components are no longer limited to basic surfactants of both hydrophobic and hydrophilic portions. Various other kinds of molecules have been used to create functional thin films at the air/liquid interface. For example, when functional molecules lacking alkyl chains are employed in some cases, the molecules pack together at the interface through weak interactions such as π - π^* and van der Waals interactions. In contrast, other stronger interactions such as coordination, covalent, and multiple hydrogen bonds may increase the stability of the film, and the application of direct guided interactions possibly control the molecular arrangements. Makiura and colleagues synthesized a series of Cu-based coordination nanosheets at the gas/liquid interface [78,79,82,87,120] by adding a small quantity of organic precursor into the metal ions solution. In addition, Ashworth and Foster also reported a series of coordination nanosheets utilizing this method, including the use of Ni²⁺, Cu²⁺, and Co²⁺ [123]. At the same time, Lahiri *et al.* successfully fabricated a series of hexaaminobenzene-based coordination nanosheets with hexagonal honeycomb crystal structure [94]. A single layer with high dimensions could not be produced due to significant π -stacking interactions between the layers. To accelerate the evaporation of the organic solvent, a small quantity of a liquid with a low surface tension was often added to allow for a high extension on the water surface [75]. In contrast to the liquid/liquid interfacial method, gas/liquid interfacial synthesis is suitable for fabricating single- or thick-layer coordination nanosheets [124,125]. Nishihara and his co-workers fabricated single-layer coordination nanosheets by gently spreading the ligand in an organic solvent on a metal ion solution [66]. The coordination reaction between the ligands and metal ions created single-layer nanosheets at the interface after fast evaporation of the organic solvent. Bao *et al.* reported have successfully synthesized large-area films with 2-nm-thick [126] under Schiff base condensation reaction at the gas/liquid interface for 2 days. Interestingly, the thickness of the film can be easily controlled by manipulating the reaction times. In addition, another single-layer nanosheet, Ni-benzenehexathiol π -conjugated nanosheet with 0.6-nm-thick, was also successfully obtained using this method [92,127]. Porphyrin and metalloporphyrin are very stable macrocyclic π -conjugated molecules with a square-planar structure holding excellent building blocks in fabricating two-dimensional supramolecular structures. The combination of peripheral polar substituents in porphyrins and a hydrophobic macrocyclic core [128–130] is ideal for producing functional nanosheets. Qian *et al.* successfully fabricated porphyrin-based nanosheets by using 5,10,15,20-tetrakis(4-pyridyl)-21H,23H-porphyrin (H₂TPyP) and its metal-ion derivatives (MTPyP, M= Zn(II), Mn(III), Ti(IV)O) on palladium salt aqueous solutions [131].

3. Nanosheets Applications

In general, bottom-up coordination nanosheets can be categorized into two different groups [132]. The first group is conjugated coordination nanosheets such as cobalt–hexaaminobenzene metal-organic coordination polymer nanosheets (Co–HAB-NSs) as published by Li *et al.* [21], the Co–DABDT (DABDT = 2,5-diamino-1,4-benzenedithiol dihydrochloride) [133], the copper–benzenhexathiol (Cu–BHT) complex-based coordination nanosheet reported by Zhu *et al.* [134] and others. These coordination nanosheets are promising next-generation molecular electronics because of their high electrical conductivity that is derived from the π -d coupling interactions. The other group is the nonconjugated coordination nanosheet such as In_2Se_3 reported by Shi *et al.* [135] and tri(terpyridine)-based building block and iron atoms (TpPB-Fe-MSc) synthesized by Wang *et al.* [136] and others. Since some of the ligands employed in the fabrication are low-conjugated, the conductivity of the coordination nanosheets might be low due to a lack of planarity. In addition to that, the electronic structures with confined molecular orbitals and low band dispersion restricted the conductivity and applicability in electronics. The nonconjugated coordination nanosheets have also gained a new dimension in different applications such as photoactivity [137,138], transmetalation [80], electrocatalysis [139,140], electrochromism [63,86,141] and others since Schlüter *et al.* obtained the monolayer bottom-up organometallic sheets at the gas/liquid interface [45].

3.1. Electrochromic nanosheets.

Electrochromism is a term that refers to materials or devices with altered optical characteristics in a reversible and continuous manner when exposed to an alternating electric field [142]. Generally, photoelectrochemical measurements are used to characterize the electrochromic performance [143]. Optical modulation, switching speed, coloring efficiency, cycle stability, and optical memory are the primary characteristics used to assess electrochromic materials or devices [144]. Electrochromic materials are often utilized [145] in commercial display device applications such as flat panel displays [146], smart windows [147], biosensors [148], and others due to the distinct color variations. However, drawbacks such as low coloring efficiency, sluggish switching speed, and poor cycle stability hinder further improvement. Advanced research in electrochromic material was initially started when Debra S. K. and colleagues published the first report on the electrochromic tungsten trioxide (WO_3) in 1969. Under the stimulation of negative voltage, the color of the WO_3 film shifted from colorless to blue in a reversible manner [149]. Moreover, most ion storage materials such as nickel oxide [150] and Prussian blue [151] exhibit superior electrochromic performances. Coordination nanosheets often exhibit metal center electronic transitions such as d-d* transitions for transition metal-based coordination nanosheets and d-f* transitions for lanthanide metal-based coordination nanosheets. In addition, the coordination nanosheets also often exhibit both metal-to-ligand charge transfer (MLCT) and ligand-to-metal charge transfer (LMCT) absorption, in which the MLCT plays an important role for the electrochromic behavior. This is because the color responsible for the MLCT may be changed in response to changes in redox states of the metal ions [152,153]. When it comes to charging transfer processes, the MLCT refers to the charge transfer from a metal d orbital to an organic ligand π^* orbital within the coordination nanosheets molecule. In contrast, LMCT refers to the charge transfer from an organic ligand π^* orbital to a metal d orbital within the coordination

nanosheets molecule [154]. Electrochromism occurs when the M^{2+}/M^{3+} pair undergoes redox reactions under the applied alternating potential causing coordination polymer color to change reversibly. For example, coordination nanosheets consisting of Fe(II) ions and terpyridine-based ligands typically show wide light absorption in a visible range that is originated from MLCT transition [59,155,156] Xing *et al.* in a study had fabricated three novel Fe(II) coordination nanosheets in which two terpyridine moieties are linked by nonconjugated alkyl chain linkers [157]. Electrochromic materials are primarily classified into organic or inorganic groups. For example, transition metal oxides such as tungsten oxide, nickel oxide, and other similar compounds are used in inorganic electrochromic materials [158,159]. Conjugated conducting polymers and coordination polymers such as polyaniline, viologen, poly (3,4-ethylenedioxythiophene): poly (styrene sulfonate) (PEDOT: PSS), and pyridyl-based coordination nanosheets are examples of organic materials [160]. The coordination nanosheets are among the organic polymers that have received increased interest as a result of their intriguing characteristics in chemistry, physics, optoelectronics, and other fields of study. Particularly, hyperbranched coordination nanosheets show rapid electrochromic switching and better coloring efficiency than other types of organic materials [62]. However, the primary disadvantage of this class of polymers is their insolubility in the common low boiling organic solvent for spray/spin coating films. Therefore, bottom-up hyperbranched coordination nanosheets provide a method for fabricating thin films for electrochromic devices with almost limitless lateral dimension and thickness. This is done by forming a network of interconnected nanosheets as well as readily deposited onto any chosen substrate with little or no modification. Nishihara *et al.* were the first to demonstrate electrochromism in multilayer hyperbranched coordination nanosheets of Fe^{2+} and Co^{2+} featuring bis(terpyridine)metal(II) complex motifs [86]. Higuchi then managed to synthesize coordination nanosheets based on the tris(2,2'-bipyridine) iron(II) complex exhibiting electrochromism [141]. In addition, Zhang *et al.* also successfully synthesized multi-colored coordination nanosheets based on the terpyridine-Fe(II) complex with excellent electrochromic properties [63]. The electrochromic switching times are less than 3s, and the electrochromic cycle stabilities are excellent in all cases. However, the optical memory in coordination nanosheets-based electrochromic devices was not investigated, although it is a critical parameter in developing power-efficient electrochromic devices. Because of its high electron affinity, 2,2':6',2''-terpyridine has been extensively studied as a ligand for transition metal ions. This moiety has the potential to be employed in preparing highly stable supramolecular coordination compounds and coordination polymers such as coordination nanosheets with fascinating magnetic, electronic, and optical properties [84,141]. Terpyridine-based coordination nanosheets display different multicolor electrochromic performances attributed to both parts of triphenylamine and $[M(\text{terpyridyl})_2]$ that have their electrochromic characteristics. The electrochromic coordination nanosheets displayed a feature of a conjugated terpyridine ligand-based framework that allows facile redox conduction throughout the system. On the other hand, the porous hyperbranched structure facilitates a rapid counter ion transport resulting in short switching times. Roy and Chakraborty successfully developed and synthesized one hyperbranched bottom-up coordination nanosheet composed of a three-arm nonconjugated flexible terpyridine (3tpy)-based ligand and Fe(II) via liquid-liquid interfacial synthesis method [108]. The 3tpy-Fe nanosheet was insoluble in all solvents, indicating that the network was hyperbranched. The free-standing film at the liquid-liquid interface is transferable to various substrates, including indium tin oxide (ITO). This electrochromic material exhibited color change at a low switching time, high coloration

efficiency, and cycle durability. Besides terpyridine-based ligand, Dong *et al.* described a star-shaped thiophene derivative with a central triphenylamine core and three arms of bithiophene. This derivative demonstrates multi-color electrochromism derived from the oxidative states of the triphenylamine and quaterthiophene groups [63,161]. The liquid-liquid interfacial synthesis was employed to fabricate the terpyridine-Fe(II) complex nanosheets. The color and thickness of these nanosheets both increased with the extension of the standing period. Regardless of the thickness, all nanosheets exhibited comparable features with two typical absorption bands at 400 nm and 580 nm and a single absorption band at 480nm. These findings were similar to the previously published Fe²⁺- terpyridyl coordination compounds suggesting that the nanosheets have been successfully fabricated. Despite the lack of visual contrast, the metal complex's rapid switching time and good electrochromic stability make it a viable candidate material system for electrochromic displays.

3.2. Conductive nanosheets.

π -conjugated coordination nanosheets have many potential applications and are comparable to graphene and molybdenum disulfide that are semiconductors with high carrier mobilities. These conjugated coordination nanosheets have a high electrical conductivity due to π -d conjugation between the metal centers and a planar conjugated ligand. However, the fabrication of this coordination nanosheet has proven to be challenging for many reasons. Nonconjugated coordination nanosheets have poor conductivity due to a lack of planarity in their structure [60]. These materials' restricted conductivity and applicability in electronics were due to the localized molecular orbitals and low band dispersion in their intrinsic electronic structures. Nishihara and colleagues discovered trinuclear dithiolene metal complexes fused with a phenylene bridge in which the valences were highly delocalized between the three dithiolene rings [162]. They successfully fabricated a π -conjugated bis(dithiolene)nickel complex nanosheet (4-Ni) in a mixed-valence state [67,85] with high electrical conductivity via liquid/liquid interfacial synthesis. This nanosheet exhibited high conductivity values, and the value changes depending on the oxidation state. Liu suggested single layer bis(dithiolene)nickel complex nanosheets as the ideal first organic 2D topological insulator [127]. The topological insulator is a novel state of matter with an insulating bulk portion but metallic-phase edges (surfaces or sides). As a result, topological insulators have the potential to be used in spintronics and quantum computing devices. Generally, most topological insulators have been based on inorganic materials [163–168]. Theories anticipated the possibility of the presence of an organic topological insulator in 2D organometallic frameworks. Nevertheless, the experimental synthesis of these theoretically suggested structures has not been established [167,168] despite the discovery of the bis(dithiolene)metal complex motif consisting of two quasi-aromatic five-membered rings with excellent electrical communication [169].

3.3. Photofunctional nanosheets.

Gözlhäuser and colleagues reported the discovery of the world's first photo-functional nanosheet [170]. This was done by the self-assembled (SAM) 4'-nitro-1,1'-biphenyl-4-thiol (NBPT) on a gold surface in which SAM was then subjected to electrons to crosslink it into an approximately 1 nm thick sheet with amino and thiol sides. Various possible combinations of inorganic cations and organic anions allow the coordination of nanosheets properties to be

tailored via bottom-up self-assembly. Bis(dipyrrinato)metal(II) and tris(dipyrrinato)metal(III) complexes exhibit significant light absorption and fluorescence in the visible range of the light spectrum [171–174] that is suitable for the fabrication of supramolecular structures and coordination polymers [175,176]. By engaging the bis(dipyrrinato)zinc(II) complex motif, Sakamoto and Nishihara fabricated photo functional coordination nanosheets via interfacial techniques [66,177] comprised of a three-way dipyrrin ligand and Zn^{2+} ions. It was the first attempt that a bis(dipyrrinato)zinc(II) coordination nanosheet was used as a photo absorber in a liquid electrolyte-filled photoelectrochemical cell and successfully generated a quantum yield (ϕ) of 0.86 percent for photoelectric conversion. Later, Sakamoto *et al.* fabricated porphyrin-hybridized bis(dipyrrinato)zinc(II) complex nanosheets by substituting the dipyrrin ligand with a porphyrin-dipyrrin hybrid ligand. With the enhanced photoresponse nature of the porphyrin unit, the absorption band broadened from 450-550 nm to 400-650 nm and the photoresponse efficiency increased by 2.02 percent [65]. Due to the lack of vacant d-orbitals in zinc(II) ions, zinc(II)-based coordination nanosheets are considered as electrical insulators because of the overlap between the π -orbitals of ligands and the d-orbitals of zinc(II) ions is minimal. To overcome this issue, iron(II) ions are the most promising alternative to zinc(II) ions because of the presence of vacant d-orbitals, and more significantly, iron(II) ions are abundant in the surface crust of the Earth. Kambe *et al.* discovered that the use of a $Fe_3(THT)_2(NH_4)_3$ (THT = 2,3,6,7,10,11- triphenylenehexathiol) film in solid-state photodetectors exhibited a maximum spectral responsivity (R) as high as 4 mA W^{-1} [119]. However, large ligands in the coordination nanosheets, such as nonplanar soft ligands and THT, obstruct the charge carrier transport paths. This results in longer distances between the metal centers [119] or unevenness of the coordination nanosheets [178,179], thereby affecting the photoelectric conversion efficiencies of the nanosheets. The nanosheets are deposited onto a transparent semiconductive metal oxide electrode such as ITO or tin oxide (SnO₂) to engage as a photoanode in a photoelectric conversion system. The decorated photoanode is installed in a photoelectric conversion cell with a suitable electrolyte solution containing a sacrificial electron donor (triethanolamine (TEOA)) [180]. Since liquid electrolytes are used in these photoelectrochemical cells, some durability problems such as electrolyte leakage, corrosion of the coordination nanosheets, and electrode destruction need to be resolved before the practical application of coordination nanosheets-based photoelectric conversion systems [181]. The practical approach will comprise solid-state designs to overcome the limitations of liquid electrolyte technology. When incorporating light harvesters into solid-state electronic devices, the electrical conductivity should be considered rather than the ionic conductivity. In response to the foregoing requirements, Wang *et al.* designed a π - conjugated coordination nanosheets composed of a bis(dithiolene)iron(II) complex [FeBHT] to serve as the photoactive layer in a liquid-free photodetector by replacing the liquid electrolytes with a Spiro-OMeTAD solid-state layer known to be an efficient hole transporter [182,183]. FeBHT was fabricated via coordination reactions between benzenehexathiol (BHT) and iron(II) ammonium sulfate [$Fe(NH_4)_2(SO_4)_2$]. BHT is a rigid, small planar ligand. Many coordination nanosheets containing the BHT ligand have shown to be an outstanding electrical conductivity owing to their high coplanarities and the distance-shortening effect between the metals [134,184]. The combination of these materials improved the photoresponses of FeBHT photodetectors with a ϕ value of 5.94%. After 60 days of exposure to air, 94 percent of the photocurrent is still maintained indicating that the nanosheets employed in the laboratory study are suitable for real-world optoelectronic applications [185].

4. Outlooks and Conclusions

MONs are highly engaging polymeric materials that have gained significant interest in materials science in current decades. Beginning with studies on graphene nanosheets, researchers have expanded their interest into this area by exploring others nanosheets with burgeoning potential in electronics, photonics, optoelectronics, spintronics, magnetism, and others. This review summarizes studies on bottom-up coordination nanosheets synthesized by coordinating organic bridging ligands and metal atoms or ions. The different ligands, metal ions, and the application of each coordination nanosheet synthesized by using either gas-liquid or liquid-liquid techniques have been reviewed in Table 1. Top-down nanosheets derived from lamellar 3D crystals such as TMDs and graphene are the subject of an ongoing study in 2D materials. In contrast, bottom-up nanosheets such as coordination nanosheets are gaining tremendous attraction because of the variety and tunability of their chemical structures as well as physical and chemical characteristics [76,119]. This is because coordination nanosheets are easily fabricated through coordination reactions at liquid/liquid or gas/liquid interfaces [186,187]. Although most of the studies on coordination nanosheets focused on creating 2D crystalline structures, some recent work has defined the material's distinctive physical characteristics, including metallic conductivity, electrochromism, and photoelectric conversion. These novel findings should open the path for fast advancements in coordination nanosheets' fundamental science and engineering and their practical applications. The design of coordination nanosheets is simple, but it relies on complex techniques to create a 2D framework. Due to the many potential combinations between the organic ligand molecules and metal ions or atoms, a wide range of coordination nanosheets can be synthesized. Some have been described in this review. To date, molecule-based nanosheets, including coordination nanosheets, lack practical functioning compared to inorganic nanosheets [188,189]. We are certain that this promising area of study will get more attention since a recent study has shown the potential for many applications in the future. Great progress has been achieved in fabricating and applying various coordination nanosheets in diverse functional electronic devices. However, significant challenges remain in gaining profound insights into the structural optimization of the coordination nanosheets, elucidating underlying mechanisms, and optimizing the device performance. Coordination nanosheets, especially the ultrathin coordination nanosheets, exhibit unique properties such as high specific surface areas, an organized 1D porous channel for ion transport, and an abundance of accessible active sites exposed on the surface, making them suitable modes in functional electronic devices. To match the demand for electronic device applications, synthetic methods for fabricating ultrathin coordination nanosheets with notable properties such as high yield, high uniformity, good dispersion, and outstanding structural stability are still highly sought. In addition, the basic constituents such as organic linkers or guest molecules, width, and thickness of nanosheets also significantly affect the physical and chemical properties such as charge mobility, surface area, and conductivity [190,191]. Therefore, it is necessary to identify additional agents to control the crystal growth, such as surfactants or other small molecules that have only weak interactions with the exposed binding sites on the surface of the nanosheets and are readily washed away from the coordination nanosheets products. An accurate prediction of nanosheets' electronic properties remains a challenge. Theoretical calculation methods are greatly needed in this aspect to guide a precise design and synthesis of new coordination nanosheets before

their assembly in electrical devices to ensure the performance meets the requirements for actual devices.

Table 1. Interfacial synthesis and application of coordination nanosheets.

Techniques	Solvent	Ligand	Metal	Waiting period	λ (nm)	Application	Ref
Gas-Liquid	chloroform	Hexafunctional terpyridine (tpy)-based monomer	Fe, Co, Ni, Zn and Pb	14-18h	$\lambda = 287$ nm and $\lambda = 578$ nm	Catalytic and magnetic	[61]
Gas-Liquid	dichloromethane	three-way dipyrin ligand	zinc(II) acetate	96 h	Orange 500nm	Photoconversion	[66]
Gas-Liquid and Liquid/liquid	chloroform and water/chloroform	5,10,15,20-tetrakis(4-aminophenyl)-21H,23H-porphine (monomer 1) or 5,10,15,20-tetrakis(4-aminophenyl)-21H,23H-porphyrin-Co(II) (monomer 2) and 2,5-dihydroxyterephthalaldehyde (monomer 3)	Co	4 h	Soret (S) band at 442nm and Q bands at 526, 571 and 656 nm	electronics and energy-related applications	[76]
Gas-Liquid	a mixed solvent of chloroform and methanol	trans-5,15-diphenyl-10,20-di(4-carboxyphenyl)porphine (trans-H2DCPP) and 5,10,15,20-tetrakis[4-(4-carboxyphenylethynyl)phenyl]porphine (H2TCPEPP)	Cu(II)	Langmuir trough	500–700 nm	molecular filters and traps	[78]
Gas-Liquid	chloroform and methanol	CoTCPP and pyridine (py)	copper(II) ions	Langmuir-Blodgett and the layer-by-layer (LB-LbL) methodologies 1 to 60 min	450 nm	Nanomaterials	[79]
Gas-Liquid	chloroform/methanol	(metalloporphyrin, 5,10,15,20-tetrakis(4-carboxyphenyl)-porphyrinato-palladium(II) (PdTCPP, 1)	Cu(II)	Langmuir trough	NA	NA	[82]
Gas-Liquid	toluene/ethanol/aqueous solution	H2TCPP	Cu(II)	Langmuir trough	430 nm	nanodevices	[87]
Liquid/Liquid	dichloromethane/pyridine and metal aqueous solution	porphyrin-dipyrin hybrid ligand with 4-fold symmetry	Zn(II)	48 h	450–550 nm	Photoconversion	[65]
Gas/Liquid	DMF/chloroform/aqueous solution	2,3,6,7,10,11-triphenylenehexathiol (THT) and 2,3,6,7,10,11-triphenylenehexamine (THA)	Co, Ni	4 h	320 nm	Electrocatalytic H ₂ Production	[83]
Liquid/Liquid	dichloromethane and metal aqueous solution	1,3,5-tris[4-(2,2':6',2''-terpyridyl)phenyl]benzene	Zn(BF ₄) ₂ ZnSO ₄	120 h	340 nm	photofunctional nanomaterials	[84]
Liquid/Liquid	dichloromethane and metal	1,3,5-tris[4-(2,2':6',2''-terpyridyl)phenyl]benzene	Fe ²⁺ or Co ²⁺	24 h	578 nm	color displays and electric paper	[86]

Techniques	Solvent	Ligand	Metal	Waiting period	λ (nm)	Application	Ref
	aqueous solution	1,3,5- tris((2,2':6',2''-terpyridyl)ethynyl)benzene					
Liquid/Liquid	dichloromethane/metal aqueous solution	1,3,5-triaminobenzene-2,4,6-trithiol	Ni(acac) ₂	192 h	-	electrocatalyst for the hydrogen evolution reaction	[88]
Gas/liquid							
Liquid/Liquid	chloroform and metal aqueous solution	benzenhexathiol	Cu	24 h	-	Topological insulator	[91]
Liquid/Liquid	toluene/methanol and metal aqueous solution	1,3,5-tris-(4-carboxyphenyl)-benzene (BTB)	None (organic nanosheet)	Langmuir trough	310 nm	energy conversion and storage.	[92]
Liquid/Liquid	dichloromethane and metal aqueous solution	benzenhexathiolate	Co, Ni, Fe	24-48 h	-	electrocatalysts	[93]
Gas/liquid	deionized water and ethyl acetate	hexaaminobenzene	Ni ²⁺ , Cu ²⁺ and Co ²⁺	4 h	-	Electronic devices	[94]
Liquid/Liquid	aqueous solution/dichloromethane	bis(dithiolene)	Pd(II)	24 h	-	electronics	[69]
Liquid/Liquid	ethyl acetate/ aqueous solution	2,3,6,7,10,11-triphenylenehexathiolate	Co	120 h	-	Catalysts	[95]
Liquid/Liquid	Ammonia (aq)/ aqueous solution/ dichloromethane	1,3,5-triaminobenzene-2,4,6-trithiol	Ni ²⁺	1 h	-	Topological insulator	[75]
Liquid/Liquid	DMF/H ₂ O	paddle-wheel building blocks	Cu(II)	24 h	-	CO ₂ separation applications	[96]
Liquid/Liquid	DMF/ aqueous solution	(ndc = 1,4- naphthalene dicarboxylate; dabco = 1,4-diazabicyclo[2.2.2]- octane)	Cu(II)	24 h	-	drug delivery, biomedical imaging, sensing and gas adsorption	[97]
Liquid/Liquid	Hexanol/ aqueous solution	benzimidazole-acetate	Zn(II)	16 h – 120 h	-	gas storage, separations and catalysis.	[100]
Liquid/Liquid	DMF/ethanol/ aqueous solution	tetrakis(4-carboxyphenyl)porphyrin	Zn, Co, Cd, Cu	6 h -24 h	588 nm	fluorescent sensor	[101]
Liquid/Liquid	Dichloromethane / aqueous solution	4,4'-(p-Tolylmethylene)bis(benzene-1,2-diol), 4,4'-(Dodecane-1,1-diy)bis(benzene-1,2-diol), Synthesis of 4,4'-(Heptane-1,1-diy)bis(benzene-1,2-diol).	Fe ²⁺ , Cu ²⁺	24 h	430-680 nm and 450-720 nm	sensing, filtration membranes, and novel catalysts	[105]

Techniques	Solvent	Ligand	Metal	Waiting period	λ (nm)	Application	Ref
Liquid/Liquid	Dimethylformamide/ acetonitrile	1,4-benzenedicarboxylate	Cu ²⁺	30 s	400 nm	Nanodevices	[106]
Liquid/Liquid	Dichloromethane / aqueous solution	(4',4''''-(2-(((2,2':6',2''-terpyridin]-4'-yloxy)methyl)-2-methylpropane-1,3-diyl)bis(oxy))di-2,2':6',2''-terpyridine)	Fe ²⁺	48 h	556 nm	display device	[108]
Liquid/Liquid	Aqueous solution/toluene	Tetrakis(diethylthiocarbamate) Molybdenum (IV)	-	24 h	330 -590 nm	energy storage devices and electronics	[109]
Gas-Liquid	chloroform / methanol	anthracene-based ligands	-	Langmuir troughs	365 nm	optoelectronic devices	[117]
Gas-Liquid	aqueous solution/Dichloromethane	benzenhexathiol	Ni(II)	24 h	-	molecular electronics	[119]
Gas-Liquid	Chloroform/DMF	1,3,5-triformylphloroglucinol	-	24 h, LB trough	-	sensing, catalysis	[124]
Gas-Liquid	aqueous/organic solvent	1,3,5-triformylphloroglucinol and ethidium bromide	-	48 h	-	Gas separation	[125]
Gas-Liquid	aqueous solution	hexaaminobenzene	Co(II)	4,8,12 h		oxygen evolution	[21]
Liquid/Liquid	aqueous solution/ chloroform	2,5-diamino-1,4-benzenedithiol dihydrochloride	Co(II)	12 h	280 to 1500 nm	smart skin devices, human-machine interfaces, and wearable electronic devices	[133]
Liquid/Liquid	Dichloromethane/ aqueous solution	benzenhexathiol	Cu(II)	-	no obvious absorption in the visible region	field-effect transistor	[134]
Liquid/Liquid	aqueous solution/ Dichloromethane	1,3,5-tri(4-(2,20:60,2''-terpyridine)phenyl)benzene	Fe(II)	24 h	317 and 581 nm	energy storage and optoelectronic	[136]
Liquid/Liquid	aqueous solution/ Dichloromethane	(trans)-1,2-bis(4'-methyl-[2,2'-bipyridin]-4-yl)ethene (BP1) and 1,4-bis((trans)-2-(4'-methyl-[2,2'-bipyridin]-4-yl)vinyl)benzene	Fe(II)	24 h	590 nm	electrochromic materials	[141]
Liquid/Liquid	aqueous solution/ Dichloromethane	1,3,5-tris(1,10-phenanthrolyl)benzene	Fe(II)	6 h	518 nm	electrochromic materials	[156]
Liquid/Liquid	aqueous solution/ Dichloromethane	benzenhexathiol	Ni(II)	-	<450 nm	OLED	[184]
Liquid/Liquid	aqueous solution/ Dichloromethane	benzenhexathiol	Fe(II)	-	365 nm	Photodetector	[185]

Funding

This research was funded by the Research Management and Innovation Centre (RMIC), Universiti Pendidikan Sultan Idris (UPSI) for the University Research Grants-GGPU (code: 2018-0080-106-01); University Research Grants-GPU (code: 2018-0143-101-01) and the Ministry of Higher Education, Malaysia for the Fundamental Research Grant Scheme for Research Acculturation of Early Career Researchers-FRGS-RACER (code: 2019-0162-103-62 (RACER/1/2019/STG01/UPSI/4)).

Acknowledgments

This research has no acknowledgment.

Conflicts of Interest

The authors declare no conflict of interest.

References

1. Butler, S.Z.; Hollen, S.M.; Cao, L.; Cui, Y.; Gupta, J.A.; Gutiérrez, H.R.; Heinz, T.F.; Hong, S.S.; Huang, J.; Ismach, A.F.; Johnston-Halperin, E. Progress, challenges, and opportunities in two-dimensional materials beyond graphene. *ACS nano* **2013**, *7*, 2898-926, <https://doi.org/10.1021/nn400280c>.
2. Yuan, S.; Feng, L.; Wang, K.; Pang, J.; Bosch, M.; Lollar, C.; Sun, Y.; Qin, J.; Yang, X.; Zhang, P.; Wang, Q. Stable metal-organic frameworks: design, synthesis, and applications. *Adv Mat* **2018**, *30*, 1704303, <https://doi.org/10.1002/adma.201704303>.
3. Zhao, M.; Huang, Y.; Peng, Y.; Huang, Z.; Ma, Q.; Zhang, H. Two-dimensional metal-organic framework nanosheets: Synthesis and applications. *Chem Soc Rev* **2018**, *47*, 6267, <https://doi.org/10.1039/c8cs00268a>.
4. Liu, J.; Wöll, C. Surface-supported metal-organic framework thin films: Fabrication methods, applications, and challenges. *Chem Soc Rev* **2017**, *46*, 5730, <https://doi.org/10.1039/c7cs00315c>.
5. Cao, L.; Lin, Z.; Peng, F.; Wang, W.; Huang, R.; Wang, C.; Yan, J.; Liang, J.; Zhang, Z.; Zhang, T.; Long, L. Self-supporting metal-organic layers as single-site solid catalysts. *Angew Chemie* **2016**, *55*, 4962-4966, <https://doi.org/10.1002/anie.201512054>.
6. Zhang, Y.; Lv, Q.; Chi, K.; Li, Q.; Fan, H.; Cai, B.; Xiao, F.; Wang, S.; Wang, Z.; Wang, L. Hierarchical porous carbon heterojunction flake arrays derived from metal organic frameworks and ionic liquid for H₂O₂ electrochemical detection in cancer tissue. *Nano Res* **2021**, *14*, 1335-1343, <https://doi.org/10.1007/s12274-020-3176-z>.
7. Park, M.; Kim, N.; Lee, J.; Gu, M.; Kim, B.S. Versatile graphene oxide nanosheets: Via covalent functionalization and their applications. *Mater Chem Front* **2021**, *5*, 4424-4444, <https://doi.org/10.1039/d1qm00066g>.
8. Nazir, A.; Le, H.T.T.; Nguyen, A.G.; Park, C.J. Graphene analogue metal organic framework with superior capacity and rate capability as an anode for lithium ion batteries. *Electrochim Acta* **2021**, *389*, 138750, <https://doi.org/10.1016/j.electacta.2021.138750>.
9. Ren, R.; Bi, S.; Wang, L.; Zhao, W.; Wei, D.; Li, T.; Xu, W.; Liu, M.; Wu, Y. Terpyridine-based Pd (II)/Ni (II) organometallic framework nano-sheets supported on graphene oxide—Investigating the fabrication, tuning of catalytic properties and synergetic effects. *RSC Adv* **2020**, *10*, 23080-23090, <https://doi.org/10.1039/D0RA02195D>.
10. Dong, R.; Han, P.; Arora, H.; Ballabio, M.; Karakus, M.; Zhang, Z.; Shekhar, C.; Adler, P.; Petkov, P.S.; Erbe, A.; Mannsfeld, S.C. High-mobility band-like charge transport in a semiconducting two-dimensional metal-organic framework. *Nat Mater* **2018**, *17*, 1027-1032, <https://doi.org/10.1038/s41563-018-0189-z>.
11. Li, Q.; Lu, L.; Liu, J.; Shi, W.; Cheng, P. Two-dimensional bimetallic coordination polymers as bifunctional evolved electrocatalysts for enhanced oxygen evolution reaction and urea oxidation reaction. *J Energy Chem* **2021**, <https://doi.org/10.1016/j.jechem.2021.04.015>.
12. Kutzscher, C.; Gelbert, A.; Ehrling, S.; Schenk, C.; Senkovska, I.; Kaskel, S. Amine assisted top-down delamination of the two-dimensional metal-organic framework Cu₂(bdc)₂. *Dalt Trans* **2017**, *46*, 16480-16484, <https://doi.org/10.1039/c7dt03890a>.
13. Kim, D.; Vasileiadou, E.S.; Spanopoulos, I.; Kanatzidis, M.G.; Tu, Q. In-Plane Mechanical Properties of Two-Dimensional Hybrid Organic-Inorganic Perovskite Nanosheets: Structure-Property Relationships. *ACS Appl Mater Interfaces* **2021**, *13*, 31642-31649, <https://doi.org/10.1021/acsami.1c06140>.
14. Lee, C.; Wei, X.; Kysar, J.W.; Hone, J. Measurement of the elastic properties and intrinsic strength of

- monolayer graphene. *Science* **2008**, *321*, 385-388, <https://doi.org/10.1126/science.1157996>.
15. Cheetham, A.K.; Rao, C.N.R.; Feller, R.K. Structural diversity and chemical trends in hybrid inorganic–organic framework materials. *Chem Commun* **2006**, 4780–4795, <https://doi.org/10.1039/B610264F>.
 16. Azlina, Y.; Azlan, M.N.; Suriani, A.B.; Halimah, M.K.; Umar, S.A. Optical properties of graphene oxide-coated tellurite glass for potential fiber optics. *J Non Cryst Solids* **2020**, *536*, 120000, <https://doi.org/10.1016/j.jnoncrsol.2020.120000>.
 17. Suriani, A.B.; Mohamed, A.; Alfarisa, S.; Mamat, M.H.; Ahmad, M.K.; Birowosuto, M.D.; Soga, T. Synthesis, transfer and application of graphene as a transparent conductive film: a review. *Bull Mater Sci* **2020**, *43*, 1-14, <https://doi.org/10.1007/s12034-020-02270-9>.
 18. Xu, X.; Liu, C.; Sun, Z.; Cao, T.; Zhang, Z.; Wang, E.; Liu, Z.; Liu, K. Interfacial engineering in graphene bandgap. *Chem Soc Rev* **2018**, *47*, 3059-3099, <https://doi.org/10.1039/c7cs00836h>.
 19. Liu, P.; Gao, B.; Wang, C.; Pan, S.; Zhai, Z.; Wu, T.; Liu, Y.; Zhang, J.; Lu, H. Two-dimensional quasi-nanosheets enabled by coordination-driving deposition and sequential etching. *Nanoscale* **2021**, *13*, 4758, <https://doi.org/10.1039/d0nr08620g>.
 20. Hu, B.; Wu, P. Facile synthesis of large-area ultrathin two-dimensional supramolecular nanosheets in water. *Nano Res* **2020**, *13*, 868-874, <https://doi.org/10.1007/s12274-020-2709-9>.
 21. Li, C.; Shi, L.; Zhang, L.; Chen, P.; Zhu, J.; Wang, X.; Fu, Y. Ultrathin two-dimensional π -d conjugated coordination polymer $\text{Co}_3(\text{hexaaminobenzene})_2$ nanosheets for highly efficient oxygen evolution. *J Mater Chem A* **2019**, *8*, 369-379, <https://doi.org/10.1039/c9ta10644h>.
 22. Zhu, W.; Chen, Q.; Jin, Q.; Chao, Y.; Sun, L.; Han, X.; Xu, J.; Tian, L.; Zhang, J.; Liu, T.; Liu, Z. Sonodynamic therapy with immune modulatable two-dimensional coordination nanosheets for enhanced anti-tumor immunotherapy. *Nano Res* **2020**, *14*, 212, <https://doi.org/10.1007/s12274-020-3070-8>.
 23. Safarpour, M.; Arefi-Oskoui, S.; Khataee, A. A review on two-dimensional metal oxide and metal hydroxide nanosheets for modification of polymeric membranes. *J Ind Eng Chem* **2020**, *82*, 31-41, <https://doi.org/10.1016/j.jiec.2019.11.002>.
 24. Yu, C.X.; Hu, F.L.; Song, J.G.; Zhang, J. Lou.; Liu, S.S.; Wang, B.X.; Meng, H.; Liu, L.L.; Ma, L.F. Ultrathin two-dimensional metal-organic framework nanosheets decorated with tetra-pyridyl calix[4]arene: Design, synthesis and application in pesticide detection. *Sensors Actuators, B Chem* **2020**, *310*, 127819, <https://doi.org/10.1016/j.snb.2020.127819>.
 25. Tan, C.; Liu, G.; Li, H.; Cui, Y.; Liu, Y. Ultrathin two-dimensional metal–organic framework nanosheets—an emerging class of catalytic nanomaterials. *Dalt Trans* **2020**, *49*, 11073, <https://doi.org/10.1039/D0DT01359E>.
 26. Kim, S.; Ju, M.; Lee, J.; Hwang, J.; Lee, J. Polymer Interfacial Self-Assembly Guided Two-Dimensional Engineering of Hierarchically Porous Carbon Nanosheets. *J Am Chem Soc* **2020**, *142*, 9250-9257, <https://doi.org/10.1021/jacs.0c00311>.
 27. Wang, J.; Li, N.; Xu, Y.; Pang, H. Two-Dimensional MOF and COF Nanosheets: Synthesis and Applications in Electrochemistry. *Chem - A Eur J* **2020**, *26*, 6402-6422, <https://doi.org/10.1002/chem.202000294>.
 28. Feng, J.; Li, X.; Shi, Z.; Zheng, C.; Li, X.; Leng, D.; Wang, Y.; Liu, J.; Zhu, L. 2D Ductile Transition Metal Chalcogenides (TMCs): Novel High-Performance Ag_2S Nanosheets for Ultrafast Photonics. *Adv Opt Mater* **2020**, *8*, 1901762, <https://doi.org/10.1002/adom.201901762>.
 29. Zhang, M.; Liu, Y.; Liu, B.; Chen, Z.; Xu, H.; Yan, K. Trimetallic NiCoFe-Layered Double Hydroxides Nanosheets Efficient for Oxygen Evolution and Highly Selective Oxidation of Biomass-Derived 5-Hydroxymethylfurfural. *ACS Catal* **2020**, *10*, 5179-5189, <https://doi.org/10.1021/acscatal.0c00007>.
 30. Kou, Z.; Wang, T.; Gu, Q.; Xiong, M.; Zheng, L.; Li, X.; Pan, Z.; Chen, H.; Verpoort, F.; Cheetham, A.K.; Mu, S.; Wang, J. Rational Design of Holey 2D Nonlayered Transition Metal Carbide/Nitride Heterostructure Nanosheets for Highly Efficient Water Oxidation. *Adv Energy Mater* **2019**, *9*, 1803768, <https://doi.org/10.1002/aenm.201803768>.
 31. Makaremi, M.; Mortazavi, B.; Rabczuk, T.; Ozin, G.A.; Singh, C.V. Theoretical Investigation: 2D N-Graphdiyne Nanosheets as Promising Anode Materials for Li/Na Rechargeable Storage Devices. *ACS Appl Nano Mater* **2018**, *2*, 127–135, <https://doi.org/10.1021/ACSANM.8B01751>.
 32. Bagheri, B.; Zarghami Dehaghani, M.; Karami, Z.; Salmankhani, A.; Rostamiyan, Y.; Zarrintaj, P.; Mashhadzadeh, A.H.; Saeb, M.R. Correlation between surface topological defects and fracture mechanism of γ -graphyne-like boron nitride nanosheets. *Comput Mater Sci* **2021**, *188*, 110152, <https://doi.org/10.1016/j.commatsci.2020.110152>.
 33. Zhang, Y.; Wang, S.; Chen, S.; Zhang, Q.; Wang, X.; Zhu, X.; Zhang, X.; Xu, X.; Yang, T.; He, M.; Yang, X.; Li, Z.; Chen, X.; Wu, M.; Lu, Y.; Ma, R.; Lu, W. Wavelength-Tunable Mid-Infrared Lasing from Black Phosphorus Nanosheets. *Adv Mater* **2020**, *32*, 1808319, <https://doi.org/10.1002/adma.201808319>.
 34. Liu, Y.-T.; Zhang, P.; Sun, N.; Anasori, B.; Zhu, Q.-Z.; Liu, H.; Gogotsi, Y.; Xu, B. Self-assembly of transition metal oxide nanostructures on MXene nanosheets for fast and stable lithium storage. *Adv Mater* **2018**, *30*, 1707334, <https://doi.org/10.1002/adma.201707334>.
 35. Li, C.; Kang, J.; Xie, J.; Wang, Y.; Zhou, L.; Hu, H.; Li, X.; He, J.; Wang, B.; Zhang, H. Two-dimensional mono-elemental germanene nanosheets: facile preparation and optoelectronic applications. *J Mater Chem C* **2020**, *8*, 16318–16325, <https://doi.org/10.1039/D0TC03892J>.

36. Sakaushi, K.; Nishihara, H. Two-Dimensional π -Conjugated Frameworks as a Model System to Unveil a Multielectron-Transfer-Based Energy Storage Mechanism. *Acc Chem Res* **2021**, *54*, 3003–3015, <https://doi.org/10.1021/ACS.ACCOUNTS.1C00172>.
37. Selvaggio, G.; Chizhik, A.; Nißler, R.; Kuhlemann, Ilyas.; Meyer, D.; Vuong, L.; Preiß, H.; Herrmann, N.; Mann, F.A.; Lv, Z.; Oswald, T.A.; Spreinat, A. Exfoliated near infrared fluorescent silicate nanosheets for (bio) photonics. *Nat Commun* **2020**, *11*, 1–11, <https://doi.org/10.1038/s41467-020-15299-5>.
38. Liu, G.; Bao, X.; Dong, W.; Wei, Q.; Mu, H.; Zhu, W.; Wang, B.; Li, J.; Shabbir, B.; Huang, Y.; Xing, G. Two-Dimensional $\text{Bi}_2\text{Sr}_2\text{CaCu}_2\text{O}_{8+\delta}$ Nanosheets for Ultrafast Photonics and Optoelectronics. *ACS Nano* **2021**, *15*, 8919–8929, <https://doi.org/10.1021/ACS.NANO.1C01567>.
39. Yang, Y.; Liu, C.; Xu, X.; Meng, Z.; Tong, W.; Ma, Z.; Zhou, C.; Sun, Y.; Sheng, Z. Antiferromagnetism in two-dimensional polyradical nanosheets. *Polym Chem* **2018**, *9*, 5499–5503, <https://doi.org/10.1039/C8PY01287C>.
40. Hwang, D.Y.; Choi, K.H.; Park, J.E.; Suh, D.H. Evolution of magnetism by rolling up hexagonal boron nitride nanosheets tailored with superparamagnetic nanoparticles. *Phys Chem Chem Phys* **2017**, *19*, 4048–4055, <https://doi.org/10.1039/C6CP08353F>.
41. Pan, Q.; Chen, X.; Liu, H.; Gan, W.; Ding, N.; Zhao, Y. Crystalline porphyrin-based graphdiyne for electrochemical hydrogen and oxygen evolution reactions. *Mater Chem Front* **2021**, *5*, 4596–4603, <https://doi.org/10.1039/D1QM00285F>.
42. Liu, Y.; Duan, X.; Huang, Y.; Duan, X. Two-dimensional transistors beyond graphene and TMDCs. *Chem Soc Rev* **2018**, *47*, 6388–6409, <https://doi.org/10.1039/C8CS00318A>.
43. Peimyoo, N.; Li, J.; Shang, J.; Shen, X.; Qiu, C.; Xie, L.; Huang, W.; Yu, T. Photocontrolled molecular structural transition and doping in graphene. *ACS Nano* **2012**, *6*, 8878–8886, <https://doi.org/10.1021/NN302876W>.
44. Rodríguez-San-Miguel, D.; Amo-Ochoa, P.; Zamora, F. MasterChem: Cooking 2D-polymers. *Chem Commun* **2016**, *52*, 4113–4127, <https://doi.org/10.1039/c5cc10283a>.
45. Payamyar, P.; King, B.T.; Öttinger, H.C.; Schlüter, A.D. Two-dimensional polymers: Concepts and perspectives. *Chem Commun* **2016**, *52*, 18–34, <https://doi.org/10.1039/c5cc07381b>.
46. Sakamoto, J.; Van Heijst, J.; Lukin, O.; Schlüter, A.D. Two-dimensional polymers: Just a dream of synthetic chemists? *Angew Chemie - Int Ed* **2009**, *48*, 1030–1069, <https://doi.org/10.1002/anie.200801863>.
47. Varaksa, N.; Pospíšil, L.; Magnera, T.F.; Michl, J. Self-assembly of a metal-ion-bound monolayer of trigonal connectors on mercury: An electrochemical Langmuir trough. *Proc Natl Acad Sci U S A* **2002**, *99*, 5012–5017, <https://doi.org/10.1073/pnas.082098299>.
48. Hou, Y.; Liu, L.; Qiu, S.; Zhou, X.; Gui, Z.; Hu, Y. DOPO-Modified Two-Dimensional Co-Based Metal–Organic Framework: Preparation and Application for Enhancing Fire Safety of Poly(lactic acid). *ACS Appl Mater Interfaces* **2018**, *10*, 8274–8286, <https://doi.org/10.1021/ACSAMI.7B19395>.
49. Wang, X.; Chi, C.; Zhang, K.; Qian, Y.; Gupta, K.M.; Kang, Z.; Jiang, J.; Zhao, D. Reversed thermo-switchable molecular sieving membranes composed of two-dimensional metal-organic nanosheets for gas separation. *Nat Commun* **2017**, *8*, 1–10, <https://doi.org/10.1038/ncomms14460>.
50. Huang, J.; Li, Y.; Huang, R.-K.; He, C.-T.; Gong, L.; Hu, Q.; Wang, L.; Xu, Y.T.; Tian, X.Y.; Liu, S.Y.; Ye, Z.M. Electrochemical exfoliation of pillared-layer metal–organic framework to boost the oxygen evolution reaction. *Angew Chemie* **2018**, *130*, 4722–4726, <https://doi.org/10.1002/ANGE.201801029>.
51. Elder, A.C.; Aleksandrov, A.B.; Nair, S.; Orlando, T.M. Interactions on External MOF Surfaces: Desorption of Water and Ethanol from CuBDC Nanosheets. *Langmuir* **2017**, *33*, 10153–10160, <https://doi.org/10.1021/ACS.LANGMUIR.7B01987>.
52. Li, Y.-N.; Wang, S.; Zhou, Y.; Bai, X.-J.; Song, G.-S.; Zhao, X.-Y.; Wang, T.Q.; Qi, X.; Zhang, X.M.; Fu, Y. Fabrication of metal–organic framework and infinite coordination polymer nanosheets by the spray technique. *Langmuir* **2017**, *33*, 1060–1065, <https://doi.org/10.1021/ACS.LANGMUIR.6B04353>.
53. Rodenas, T.; Luz, I.; Prieto, G.; Seoane, B.; Miro, H.; Corma, A.; Kapteijn, F.; i Xamena, F.X.; Gascon, J. Metal–organic framework nanosheets in polymer composite materials for gas separation. *Nat Mater* **2014**, *14*, 48–55, <https://doi.org/10.1038/nmat4113>.
54. Lu, Q.; Zhao, M.; Chen, J.; Chen, B.; Tan, C.; Zhang, X.; Huang, Y.; Yang, J.; Cao, F.; Yu, Y.; Ping, J. *In situ* Synthesis of Metal Sulfide Nanoparticles Based on 2D Metal–Organic Framework Nanosheets. *Small* **2016**, *12*, 4669–4674, <https://doi.org/10.1002/SMLL.201600976>.
55. Ding, Y.; Chen, Y.-P.; Zhang, X.; Chen, L.; Dong, Z.; Jiang, H.-L.; Xu, H.; Zhou, H.C. Controlled intercalation and chemical exfoliation of layered metal–organic frameworks using a chemically labile intercalating agent. *J Am Chem Soc* **2017**, *139*, 9136–9139, <https://doi.org/10.1021/JACS.7B04829>.
56. Ye, L.; Gao, Y.; Cao, S.; Chen, H.; Yao, Y.; Hou, J.; Sun, L. Assembly of highly efficient photocatalytic CO_2 conversion systems with ultrathin two-dimensional metal–organic framework nanosheets. *Appl Catal B Environ* **2018**, *227*, 54–60, <https://doi.org/10.1016/J.APCATB.2018.01.028>.
57. Wang, Y.; Zhao, M.; Ping, J.; Chen, B.; Cao, X.; Huang, Y.; Tan, C.; Ma, Q.; Wu, S.; Yu, Y.; Lu, Q. Bioinspired design of ultrathin 2D bimetallic metal–organic-framework nanosheets used as biomimetic enzymes. *Adv Mater* **2016**, *28*, 4149–4155, <https://doi.org/10.1002/ADMA.201600108>.
58. Kondo, A.; Tiew, C.C.; Moriguchi, F.; Maeda, K. Fabrication of metal–organic framework nanosheets and

- nanorolls with N-donor type bridging ligands. *Dalt Trans* **2013**, *42*, 15267–15270, <https://doi.org/10.1039/C3DT52130C>.
59. Schott, M.; Niklaus, L.; Clade, J.; Posset, U. Electrochromic metallo-supramolecular polymers showing visible and near-infrared light transmittance modulation. *Sol Energy Mater Sol Cells* **2019**, *200*, 110001, <https://doi.org/10.1016/j.solmat.2019.110001>.
60. Bauer, T.; Zheng, Z.; Renn, A.; Enning, R.; Stemmer, A.; Sakamoto, J.; Schlüter, A.D. Synthesis of free-standing, monolayered organometallic sheets at the air/water interface. *Angew Chemie Int Ed* **2011**, *50*, 7879–7884, <https://doi.org/10.1002/ANIE.201100669>.
61. Zheng, Z.; Ruiz-Vargas, C.S.; Bauer, T.; Rossi, A.; Payamyar, P.; Schütz, A.; Stemmer, A.; Sakamoto, J.; Schlüter, A.D. Square-Micrometer-Sized, Free-Standing Organometallic Sheets and Their Square-Centimeter-Sized Multilayers on Solid Substrates. *Macromol Rapid Commun* **2013**, *34*, 1670–1680, <https://doi.org/10.1002/MARC.201300624>.
62. Hu, C.W.; Sato, T.; Zhang, J.; Moriyama, S.; Higuchi, M. Three-dimensional Fe(II)-based metallo-supramolecular polymers with electrochromic properties of quick switching, large contrast, and high coloration efficiency. *ACS Appl Mater Interfaces* **2014**, *6*, 9118–9125, <https://doi.org/10.1021/am5010859>.
63. Kuai, Y.; Li, W.; Dong, Y.; Wong, W.Y.; Yan, S.; Dai, Y.; Zhang, C. Multi-color electrochromism from coordination nanosheets based on a terpyridine-Fe (II) complex. *Dalt Trans* **2019**, *48*, 15121–15126, <https://doi.org/10.1039/c9dt02980j>.
64. Zheng, Z.; Opilik, L.; Schiffmann, F.; Liu, W.; Bergamini, G.; Ceroni, P.; Lee, L.T.; Schütz, A.; Sakamoto, J.; Zenobi, R.; VandeVondele, J. Synthesis of two-dimensional analogues of copolymers by site-to-site transmetalation of organometallic monolayer sheets. *J Am Chem Soc* **2014**, *136*, 6103–6110, <https://doi.org/10.1021/JA501849Y>.
65. Sakamoto, R.; Yagi, T.; Hoshiko, K.; Kusaka, S.; Matsuoka, R.; Maeda, H.; Liu, Z.; Liu, Q.; Wong, W.Y.; Nishihara, H. Photofunctionality in Porphyrin-Hybridized Bis (dipyrrinato) zinc (II) Complex Micro-and Nanosheets. *Angew Chemie - Int Ed* **2017**, *56*, 3526–3530, <https://doi.org/10.1002/anie.201611785>.
66. Sakamoto, R.; Hoshiko, K.; Liu, Q.; Yagi, T.; Nagayama, T.; Kusaka, S.; Tsuchiya, M.; Kitagawa, Y.; Wong, W.Y.; Nishihara, H. A photofunctional bottom-up bis (dipyrrinato) zinc (II) complex nanosheet. *Nat Commun* **2015**, *6*, 1–9, <https://doi.org/10.1038/ncomms7713>.
67. Hoshiko, K.; Kambe, T.; Sakamoto, R.; Takada, K.; Nishihara, H. Fabrication of dense and multilayered films of a nickel bis(dithiolene) nanosheet by means of the langmuirschäfer method. *Chem Lett* **2014**, *43*, 252–253, <https://doi.org/10.1246/cl.130882>.
68. Chen, I.-F.; Lu, C.-F.; Su, W.-F. Highly Conductive 2D Metal–Organic Framework Thin Film Fabricated by Liquid–Liquid Interfacial Reaction Using One-Pot-Synthesized Benzenehexathiol. *Langmuir* **2018**, *34*, 15754–15762, <https://doi.org/10.1021/ACS.LANGMUIR.8B03938>.
69. Pal, T.; Kambe, T.; Kusamoto, T.; Foo, M.L.; Matsuoka, R.; Sakamoto, R.; Nishihara, H. Interfacial synthesis of electrically conducting palladium bis (dithiolene) complex nanosheet. *Chempluschem* **2015**, *80*, 1255–1258, <https://doi.org/10.1002/CPLU.201500206>.
70. Dong, R.; Pfeiffermann, M.; Liang, H.; Zheng, Z.; Zhu, X.; Zhang, J.; Feng, X. Large-area, free-standing, two-dimensional supramolecular polymer single-layer sheets for highly efficient electrocatalytic hydrogen evolution. *Angew Chemie Int Ed* **2015**, *54*, 12058–12063, <https://doi.org/10.1002/ANIE.201506048>.
71. Abhervé, A.; Mroweh, N.; Cauchy, T.; Pop, F.; Cui, H.; Kato, R.; Vanthuyne, N.; Alemany, P.; Canadell, E.; Avarvari, N. Conducting chiral nickel (ii) bis (dithiolene) complexes: structural and electron transport modulation with the charge and the number of stereogenic centres. *J Mater Chem C* **2021**, *9*, 4119–4140, <https://doi.org/10.1039/d1tc00439e>.
72. Sheberla, D.; Sun, L.; Blood-Forsythe, M.A.; Er, S.; Wade, C.R.; Brozek, C.K.; Aspuru-Guzik, A.; Dincă, M. High electrical conductivity in Ni₃(2, 3, 6, 7, 10, 11-hexaiminotriphenylene)₂, a semiconducting metal–organic graphene analogue. *J Am Chem Soc* **2014**, *136*, 8859–8862, <https://doi.org/10.1021/JA502765N>.
73. Campbell, M.G.; Sheberla, D.; Liu, S.F.; Swager, T.M.; Dincă, M. Cu₃(hexaiminotriphenylene)₂: an electrically conductive 2D metal–organic framework for chemiresistive sensing. *Angew Chem Int Ed Engl* **2015**, *54*, 4349–4352, <https://doi.org/10.1002/ANIE.201411854>.
74. Chen, S.; Dai, J.; Zeng, X.C. Metal–organic Kagome lattices M₃(2,3,6,7,10,11-hexaiminotriphenylene)₂ (M = Ni and Cu): from semiconducting to metallic by metal substitution. *Phys Chem Chem Phys* **2015**, *17*, 5954–5958, <https://doi.org/10.1039/C4CP05328A>.
75. Sun, X.; Wu, K.-H.; Sakamoto, R.; Kusamoto, T.; Maeda, H.; Nishihara, H. Conducting π -Conjugated Bis(iminothiolato)nickel Nanosheet. *Chem Lett* **2017**, *46*, 1072–1075, <https://doi.org/10.1246/CL.170382>.
76. Sahabudeen, H.; Qi, H.; Glatz, B.A.; Tranca, D.; Dong, R.; Hou, Y.; Zhang, T.; Kuttner, C.; Lehnert, T.; Seifert, G.; Kaiser, U. Wafer-sized multifunctional polyimine-based two-dimensional conjugated polymers with high mechanical stiffness. *Nat Commun* **2016**, *7*, 1–8, <https://doi.org/10.1038/ncomms13461>.
77. Doryab, A.; Taskin, M.B.; Stahlhut, P.; Schröppel, A.; Orak, S.; Voss, C.; Ahluwalia, A.; Rehberg, M.; Hilgendorff, A.; Stöger, T.; Groll, J. A Bioinspired *in vitro* Lung Model to Study Particokinetics of Nano-/Microparticles Under Cyclic Stretch and Air-Liquid Interface Conditions. *Front Bioeng Biotechnol* **2021**, *9*, 616830, <https://doi.org/10.3389/fbioe.2021.616830>.
78. Makiura, R.; Usui, R.; Sakai, Y.; Nomoto, A.; Ogawa, A.; Sakata, O.; Fujiwara, A. Towards rational

- modulation of in-plane molecular arrangements in metal-organic framework nanosheets. *Chempluschem* **2014**, *79*, 1352–1360, <https://doi.org/10.1002/cplu.201402150>.
79. Makiura, R.; Tsuchiyama, K.; Sakata, O. Self-assembly of highly crystalline two-dimensional MOF sheets on liquid surfaces. *CrystEngComm* **2011**, *13*, 5538–5541, <https://doi.org/10.1039/C1CE05684K>.
80. Li, X.; Lin, X.; Lin, S.; Zhou, S.; Fang, G.; Zhao, H.; Wang, L.; Cong, S. From Dilute to Multiple Layers: Bottom-Up Self-Assembly of Rough Gold Nanorods as SERS Platform for Quantitative Detection of Thiram in Soil. *Adv Mater Interfaces* **2021**, *8*, 2100412, <https://doi.org/10.1002/admi.202100412>.
81. Bielejewska, N.; Hertmanowski, R. Functionalization of LC molecular films with nanocrystalline cellulose: A study of the self-assembly processes and molecular stability. *Colloids Surf B Biointerfaces* **2020**, *187*, 110634, <https://doi.org/10.1016/j.colsurfb.2019.110634>.
82. Makiura, R.; Kononov, O. Interfacial growth of large-area single-layer metal-organic framework nanosheets. *Sci Rep* **2013**, *3*, 1, <https://doi.org/10.1038/SREP02506>.
83. Dong, R.; Zheng, Z.; Tranca, D.C.; Zhang, J.; Chandrasekhar, N.; Liu, S.; Zhuang, X.; Seifert, G.; Feng, X. Immobilizing molecular metal dithiolene–diamine complexes on 2D metal–organic frameworks for electrocatalytic H₂ production. *Chem – A Eur J* **2017**, *23*, 2255–2260, <https://doi.org/10.1002/CHEM.201605337>.
84. Tsukamoto, T.; Takada, K.; Sakamoto, R.; Matsuoka, R.; Toyoda, R.; Maeda, H.; Yagi, T.; Nishikawa, M.; Shinjo, N.; Amano, S.; Iokawa, T. Coordination nanosheets based on terpyridine–zinc (II) complexes: as photoactive host materials. *J Am Chem Soc* **2017**, *139*, 5359–5566, <https://doi.org/10.1021/jacs.6b12810>.
85. Kambe, T.; Kusamoto, T.; Sakamoto, R.; Nishihara, H. Modulation of electronic state of π -conjugated nickelladithiolene complex nanosheet. In *Macromolecular Symposia*, 2nd ed.; Meyer, S., Huesmann, D., Pfisterer, A., Staffilani, M., Weng, B., Eds.; Publisher: Wiley-VCH Verlag, Weinheim, **2015**, *351*, 78–80, <https://doi.org/10.1002/masy.201300127>.
86. Takada, K.; Sakamoto, R.; Yi, S.T.; Katagiri, S.; Kambe, T.; Nishihara, H. Electrochromic Bis(terpyridine)metal Complex Nanosheets. *J Am Chem Soc* **2015**, *137*, 4681–4689, <https://doi.org/10.1021/ja510788b>.
87. Motoyama, S.; Makiura, R.; Sakata, O.; Kitagawa, H. Highly Crystalline Nanofilm by Layering of Porphyrin Metal–Organic Framework Sheets. *J Am Chem Soc* **2011**, *133*, 5640–5643, <https://doi.org/10.1021/JA110720F>.
88. Sun, X.; Wu, K.H.; Sakamoto, R.; Kusamoto, T.; Maeda, H.; Ni, X.; Jiang, W.; Liu, F.; Sasaki, S.; Masunaga, H.; Nishihara, H. Bis (aminothiolato) nickel nanosheet as a redox switch for conductivity and an electrocatalyst for the hydrogen evolution reaction. *Chem Sci* **2017**, *8*, 8078–8085, <https://doi.org/10.1039/c7sc02688a>.
89. Maed, H.; Sakamoto, R.; Nishihara, H. Coordination Programming of Two-Dimensional Metal Complex Frameworks. *Langmuir* **2016**, *32*, 2527–2238, <https://doi.org/10.1021/ACS.LANGMUIR.6B00156>.
90. Tang, L.P.; Yang, S.; Liu, D.; Wang, C.; Ge, Y.; Tang, L.M.; Zhou, R.L.; Zhang, H. Two-dimensional porous coordination polymers and nano-composites for electrocatalysis and electrically conductive applications. *J Mater Chem A* **2020**, *8*, 14356–14383, <https://doi.org/10.1039/d0ta03356a>.
91. Huang, X.; Zhang, S.; Liu, L.; Yu, L.; Chen, G.; Xu, W.; Zhu, D. Superconductivity in a Copper (II)-Based Coordination Polymer with Perfect Kagome Structure. *Angew Chemie* **2018**, *130*, 152–156, <https://doi.org/10.1002/ange.201707568>.
92. Makiura, R.; Tsuchiyama, K.; Pohl, E.; Prassides, K.; Sakata, O.; Tajiri, H.; Kononov, O. Air/Liquid Interfacial Nanoassembly of Molecular Building Blocks into Preferentially Oriented Porous Organic Nanosheet Crystals via Hydrogen Bonding. *ACS Nano* **2017**, *11*, 10875–10882, <https://doi.org/10.1021/ACSNANO.7B04447>.
93. Downes, C.A.; Clough, A.J.; Chen, K.; Yoo, J.W.; Marinescu, S.C. Evaluation of the H₂ Evolving Activity of Benzenehexathiolate Coordination Frameworks and the Effect of Film Thickness on H₂ Production. *ACS Appl Mater Interfaces* **2018**, *10*, 1719–1727, <https://doi.org/10.1021/ACSAMI.7B15969>.
94. Lahiri, N.; Lotfzadeh, N.; Tsuchikawa, R.; Deshpande, V. V.; Louie, J. Hexaaminobenzene as a building block for a family of 2D coordination polymers. *J Am Chem Soc* **2017**, *139*, 2119, <https://doi.org/10.1021/jacs.6b09889>.
95. Clough, A.J.; Skelton, J.M.; Downes, C.A.; Rosa, A.A. de la.; Yoo, J.W.; Walsh, A.; Melot, B.C.; Marinescu, S.C. Metallic conductivity in a two-dimensional cobalt dithiolene metal–organic framework. *J Am Chem Soc* **2017**, *139*, 10863–10867, <https://doi.org/10.1021/JACS.7B05742>.
96. Zha, J.; Zhang, X. Room-Temperature Synthesis of Two-Dimensional Metal–Organic Frameworks with Controllable Size and Functionality for Enhanced CO₂ Sorption. *Cryst Growth Des* **2018**, *18*, 3209–3214, <https://doi.org/10.1021/ACS.CGD.8B00349>.
97. Pham, M.-H.; Vuong, G.-T.; Fontaine, F.-G.; Do, T.-O. Rational Synthesis of Metal–Organic Framework Nanocubes and Nanosheets Using Selective Modulators and Their Morphology-Dependent Gas-Sorption Properties. *Cryst Growth Des* **2012**, *12*, 3091–3095, <https://doi.org/10.1021/CG300297P>.
98. Yuan, Y.; Wang, W.; Qiu, L.; Peng, F.; Jiang, X.; Xie, A.; Shen, Y.; Tian, X.; Zhang, L. Surfactant-assisted facile synthesis of fluorescent zinc benzenedicarboxylate metal-organic framework nanorods with enhanced nitrobenzene explosives detection. *Mater Chem Phys* **2011**, *131*, 358–361,

- <https://doi.org/10.1016/J.MATCHEMPHYS.2011.09.056>.
99. Barati Darband, G.; Aliofkhaezai, M.; Hyun, S.; Sabour Rouhaghdam, A.; Shanmugam, S. Electrodeposition of Ni-Co-Fe mixed sulfide ultrathin nanosheets on Ni nanocones: A low-cost, durable and high performance catalyst for electrochemical water splitting. *Nanoscale* **2019**, *11*, 16621-16634, <https://doi.org/10.1039/c9nr04529e>.
 100. Xue, F.; Kumar, P.; Xu, W.; Mkhoyan, K.A.; Tsapatsis, M. Direct Synthesis of 7 nm-Thick Zinc(II)-Benzimidazole-Acetate Metal-Organic Framework Nanosheets. *Chem Mater* **2017**, *30*, 69-73, <https://doi.org/10.1021/ACS.CHEMMATER.7B04083>.
 101. Zhao, M.; Wang, Y.; Ma, Q.; Huang, Y.; Zhang, X.; Ping, J.; Zhang, Z.; Lu, Q.; Yu, Y.; Xu, H.; Zhao, Y. Ultrathin 2D metal-organic framework nanosheets. *Adv Mater* **2015**, *27*, 7372-7378, <https://doi.org/10.1002/ADMA.201503648>.
 102. Shang, W.; Kang, X.; Ning, H.; Zhang, J.; Zhang, X.; Wu, Z.; Mo, G.; Xing, X.; Han, B. Shape and size controlled synthesis of MOF nanocrystals with the assistance of ionic liquid microemulsions. *Langmuir* **2013**, *29*, 13168-13174, <https://doi.org/10.1021/LA402882A>.
 103. Ameloot, R.; Vermoortele, F.; Vanhove, W.; Roeffaers, M.B.J.; Sels, B.F.; De Vos, D.E. Interfacial synthesis of hollow metal-organic framework capsules demonstrating selective permeability. *Nat Chem* **2011**, *3*, 382-387, <https://doi.org/10.1038/nchem.1026>.
 104. Biswal, B.P.; Bhaskar, A.; Banerjee, R.; Kharul, U.K. Selective interfacial synthesis of metal-organic frameworks on a polybenzimidazole hollow fiber membrane for gas separation. *Nanoscale* **2015**, *7*, 7291-7298, <https://doi.org/10.1039/c5nr00299k>.
 105. Joshi, S.; Kathuria, H.; Verma, S.; Valiyaveetil, S. Functional Catechol-Metal Polymers via Interfacial Polymerization for Applications in Water Purification. *ACS Appl Mater Interfaces* **2020**, *12*, 19044-19053, <https://doi.org/10.1021/acsami.0c03133>.
 106. Bai XJ, Chen D, Li LL, Shao L, He WX, Chen H, Li YN, Zhang XM, Zhang LY, Wang TQ, Fu Y. Fabrication of MOF thin films at miscible liquid-liquid interface by spray method. *ACS Appl Mater Interfaces* **2018**, *10*, 25960-25966, <https://doi.org/10.1021/acsami.8b09812>.
 107. Arai, R.; Li, M.; Toyoda, R.; Maeda, H.; Nishihara, H. Redox-active, luminescent coordination nanosheet capsules containing magnetite. *Sci Rep* **2020**, *10*, 1-7, <https://doi.org/10.1038/s41598-020-70715-6>.
 108. Roy, S.; Chakraborty, C. Interfacial Coordination Nanosheet Based on Nonconjugated Three-Arm Terpyridine: A Highly Color-Efficient Electrochromic Material to Converge Fast Switching with Long Optical Memory. *ACS Appl Mater Interfaces* **2020**, *12*, 35181-35192, <https://doi.org/10.1021/acsami.0c06045>.
 109. Higgins, E.P.C.; McAdams, S.G.; Hopkinson, D.G.; Byrne, C.; Walton, A.S.; Lewis, D.J.; Dryfe, R.A. Room-Temperature Production of Nanocrystalline Molybdenum Disulfide (MoS₂) at the Liquid-Liquid Interface. *Chem Mater* **2019**, *31*, 5384-5391, <https://doi.org/10.1021/acs.chemmater.8b05232>.
 110. Li, Y.; Zhang, M.; Guo, X.; Wen, R.; Li, X.; Li, X.; Li, S.; Ma, L. Growth of high-quality covalent organic framework nanosheets at the interface of two miscible organic solvents. *Nanoscale Horizons* **2018**, *3*, 205-212, <https://doi.org/10.1039/c7nh00172j>.
 111. Wang, W.; Zhao, W.; Xu, H.; Liu, S.; Huang, W.; Zhao, Q. Fabrication of ultra-thin 2D covalent organic framework nanosheets and their application in functional electronic devices. *Coord Chem Rev* **2021**, *429*, 213616, <https://doi.org/10.1016/j.ccr.2020.213616>.
 112. Hao, Q.; Zhao, C.; Sun, B.; Lu, C.; Liu, J.; Liu, M.; Wan, L.J.; Wang, D. Confined synthesis of two-dimensional covalent organic framework thin films within superspreading water layer. *J Am Chem Soc* **2018**, *140*, 12152-12158, <https://doi.org/10.1021/jacs.8b07120>.
 113. Dey, K.; Pal, M.; Rout, K.C.; Kunjattu, S.S.; Das, A.; Mukherjee, R.; Kharul, U.K.; Banerjee, R. Selective molecular separation by interfacially crystallized covalent organic framework thin films. *J Am Chem Soc* **2017**, *139*, 13083-13091, <https://doi.org/10.1021/jacs.7b06640>.
 114. Zarbin, A.J.G. Liquid-liquid interfaces: a unique and advantageous environment to prepare and process thin films of complex materials. *Mater Horizons* **2021**, *8*, 1409-1432, <https://doi.org/10.1039/d0mh01676d>.
 115. Mehl, H.; Oliveira, M.M.; Zarbin, A.J.G. Thin and transparent films of graphene/silver nanoparticles obtained at liquid-liquid interfaces: Preparation, characterization and application as SERS substrates. *J Colloid Interface Sci* **2015**, *438*, 29-38, <https://doi.org/10.1016/j.jcis.2014.09.068>.
 116. Wells, R.A.; Johnson, H.; Lhermitte, C.R.; Kinge, S.; Sivula, K. Roll-to-Roll Deposition of Semiconducting 2D Nanoflake Films of Transition Metal Dichalcogenides for Optoelectronic Applications. *ACS Appl Nano Mater* **2019**, *2*, 7705-7712, <https://doi.org/10.1021/ACSANM.9B01774>.
 117. Müller, V.; Hungerland, T.; Baljovic, M.; Jung, T.; Spencer, N.D.; Eghlidi, H.; Payamyar, P.; Schlüter, A.D. Ink-Free Reversible Optical Writing in Monolayers by Polymerization of a Trifunctional Monomer: Toward Rewritable "Molecular Paper". *Adv Mater* **2017**, *29*, 1701220, <https://doi.org/10.1002/adma.201701220>.
 118. Znamenskaya Falk, Y.; Schmitt, J.; Alfredsson, V. Langmuir - Blodgett monolayers of SBA-15 particles with different morphologies. *Microporous Mesoporous Mater* **2018**, *256*, 32-38, <https://doi.org/10.1016/j.micromeso.2017.07.049>.
 119. Kambe T, Sakamoto R, Hoshiko K, Takada K, Miyachi M, Ryu JH, Sasaki S, Kim J, Nakazato K, Takata M,

- Nishihara H. π -Conjugated nickel bis (dithiolene) complex nanosheet. *J Am Chem Soc* **2013**, *135*, 2462–2465, <https://doi.org/10.1021/ja312380b>.
120. Makiura, R.; Motoyama, S.; Umemura, Y.; Yamanaka, H.; Sakata, O.; Kitagawa, H. Surface nano-architecture of a metal–organic framework. *Nat Mater* **2010**, *9*, 565–571, <https://doi.org/10.1038/nmat2769>.
121. Park, J.H.; Culp, J.T.; Hall, D.W.; Talham, D.R.; Meisel, M.W. Magnetic properties of a two-dimensional mixed-spin system. *Phys B Condens Matter* **2003**, *329*, 1152–1153, [https://doi.org/10.1016/S0921-4526\(02\)02053-7](https://doi.org/10.1016/S0921-4526(02)02053-7).
122. Culp, J.T.; Park, J.H.; Frye, F.; Huh, Y.D.; Meisel, M.W.; Talham, D.R. Magnetism of metal cyanide networks assembled at interfaces. *Coord Chem Rev* **2005**, *249*, 2642–2648, <https://doi.org/10.1016/J.CCR.2005.05.011>.
123. Ashworth, D.J.; Foster, J.A. Metal-organic framework nanosheets (MONs): A new dimension in materials chemistry. *J Mater Chem A* **2018**, *6*, 16292–16307, <https://doi.org/10.1039/c8ta03159b>.
124. Cheng, Y.; Ravi, S.K.; Wang, Y.; Tao, J.; Gu, Y.; Tan, S.C.; Zhao, D. Covalent organic nanosheets with large lateral size and high aspect ratio synthesized by Langmuir-Blodgett method. *Chinese Chem Lett* **2018**, *29*, 869–872, <https://doi.org/10.1016/j.ccllet.2017.09.002>.
125. Ying, Y.; Tong, M.; Ning, S.; Ravi, S.K.; Peh, S.B.; Tan, S.C.; Pennycook, S.J.; Zhao, D. Ultrathin two-dimensional membranes assembled by ionic covalent organic nanosheets with reduced apertures for gas separation. *J Am Chem Soc* **2020**, *142*, 4472–4480, <https://doi.org/10.1021/jacs.9b13825>.
126. Feldblyum, J.I.; McCreery, C.H.; Andrews, S.C.; Kurosawa, T.; Santos, E.J.G.; Duong, V.; Fang, L.; Ayzner, A.L.; Bao, Z. Few-layer, large-area, 2D covalent organic framework semiconductor thin films. *Chem Commun* **2015**, *51*, 13894–13897, <https://doi.org/10.1039/c5cc04679c>.
127. Wang, Z.F.; Su, N.; Liu, F. Prediction of a two-dimensional organic topological insulator. *Nano Lett* **2013**, *13*, 2842–2845, <https://doi.org/10.1021/nl401147u>.
128. Mustafar, S.; Abbas, N.M.; Juahir, Y.; Ali, N.M.; Hashim, N.; Sharif, A.M. Characterisation of porphyrinic nanowires on three different solid substrates. *Int J Nanoelectron Mater* **2020**, *13*, 373–380.
129. Suzaliza, M.; Norliana, M.A.; Lee, Y.L.; Norhayati, H.; Illyas, M.I. A glance on immobilisation of porphyrins on solid support and potential future research. *AIP Conf Proc* **2018**, *2030*, 020100, <https://doi.org/10.1063/1.5066741>.
130. Sakamoto, R.; Mustafar, S.; Nishihara, H. Meso-N-arylamino- and N, N-diarylaminoporphyrinoids: Syntheses, properties and applications. *J Porphyr Phthalocyanines* **2015**, *19*, 21–31, <https://doi.org/10.1142/S1088424615500091>.
131. Qian, D.-J.; Nakamura, C.; Miyake, J. Layer-by-layer assembly of metal-mediated multiporphyrin arrays. *Chem Commun* **2001**, *1*, 2312–2313, <https://doi.org/10.1039/B106716H>.
132. Wang, L.; Sahabudeen, H.; Zhang, T.; Dong, R. Liquid-interface-assisted synthesis of covalent-organic and metal-organic two-dimensional crystalline polymers. *Npj 2D Mater Appl* **2018**, *2*, 26, <https://doi.org/10.1038/s41699-018-0071-5>.
133. Li, Z.; Chang, S.; Zhang, H.; Hu, Y.; Huang, Y.; An, L.; Ren, S. Two-Dimensional Conductive π -d Frameworks with Multiple Sensory Capabilities. *ACS Appl Mater Interfaces* **2021**, *13*, 28703–28709, <https://doi.org/10.1021/acsami.1c06596>.
134. Huang, X.; Sheng, P.; Tu, Z.; Zhang, F.; Wang, J.; Geng, H.; Zou, Y.; Di, C.A.; Yi, Y.; Sun, Y.; Xu, W. A two-dimensional π -d conjugated coordination polymer with extremely high electrical conductivity and ambipolar transport behaviour. *Nat Commun* **2015**, *6*, 1–8, <https://doi.org/10.1038/ncomms8408>.
135. Shi, H.; Li, M.; Shaygan Nia, A.; Wang, M.; Park, S.W.; Zhang, Z.; Lohe, M.R.; Yang, S.; Feng, X. Ultrafast Electrochemical Synthesis of Defect-Free In₂Se₃ Flakes for Large-Area Optoelectronics. *Adv Mater* **2020**, *32*, 1907244, <https://doi.org/10.1002/adma.201907244>.
136. Wang, H.; Qiu, F.; Lu, C.; Zhu, J.; Ke, C.; Han, S.; Zhuang, X. A Terpyridine-Fe²⁺-Based Coordination Polymer Film for On-Chip Micro-Supercapacitor with AC Line-Filtering Performance. *Polymers (Basel)* **2021**, *13*, 1002, <https://doi.org/10.3390/polym13071002>.
137. Pang, B.; Liu, S.; Tu, Y.; Wang, X. Controllable Synthesis and Enhanced Photoactivity of Two-Dimensional Bi₂WO₆ Ultra-Thin Nanosheets. *ChemistrySelect* **2021**, *6*, 5381–5386, <https://doi.org/10.1002/slct.202101280>.
138. Wen, Y.; Wei, F.; Xu, W.; Jiang, X.; Cui, J.; Ai, Y.; Chen, J.; Cui, A.; Hu, Z.; Fu, J.; Liu, S. Constructing polymers towards ultrathin nanosheets with dual mesopores and intrinsic photoactivity. *Chem Commun* **2020**, *56*, 3191–3194, <https://doi.org/10.1039/d0cc00292e>.
139. Miner, E.M.; Fukushima, T.; Sheberla, D.; Sun, L.; Surendranath, Y.; Dinca, M. Electrochemical oxygen reduction catalysed by Ni₃ (hexaiminotriphenylene)₂. *Nat Commun* **2016**, *7*, 1–7, <https://doi.org/10.1038/ncomms10942>.
140. Yu, M.; Dong, R.; Feng, X. Two-Dimensional Carbon-Rich Conjugated Frameworks for Electrochemical Energy Applications. *J Am Chem Soc* **2020**, *142*, 12903–12915, <https://doi.org/10.1021/jacs.0c05130>.
141. Bera, M.K.; Mori, T.; Yoshida, T.; Ariga, K.; Higuchi, M. Construction of Coordination Nanosheets Based on Tris(2,2'-bipyridine)-Iron (Fe²⁺) Complexes as Potential Electrochromic Materials. *ACS Appl Mater Interfaces* **2019**, *11*, 11893–11903, <https://doi.org/10.1021/acsami.8b22568>.
142. Wałęsa-Chorab, M.; Banasz, R.; Marcinkowski, D.; Kubicki, M.; Patroniak, V. Electrochromism and

- electrochemical properties of complexes of transition metal ions with benzimidazole-based ligand. *RSC Adv* **2017**, *7*, 50858–50867, <https://doi.org/10.1039/C7RA10451K>.
143. Cai, G.; Darmawan, P.; Cui, M.; Wang, J.; Chen, J.; Magdassi, S.; Lee, P.S. Highly stable transparent conductive silver grid/PEDOT: PSS electrodes for integrated bifunctional flexible electrochromic supercapacitors. *Adv Energy Mater* **2016**, *6*, 1501882, <https://doi.org/10.1002/AENM.201501882>.
144. Zhang, W.; Wang, X.; Wang, Y.; Yang, G.; Gu, C.; Zheng, W.; Zhang, Y.M.; Li, M.; Zhang, S.X. Bio-inspired ultra-high energy efficiency bistable electronic billboard and reader. *Nat Commun* **2019**, *10*, 1–8, <https://doi.org/10.1038/s41467-019-09556-5>.
145. Hao, Q.; Li, Z.J.; Bai, B.; Zhang, X.; Zhong, Y.W.; Wan, L.J.; Wang, D. A Covalent Organic Framework Film for Three-State Near-Infrared Electrochromism and a Molecular Logic Gate. *Angew Chemie - Int Ed* **2021**, *60*, 12498–12503, <https://doi.org/10.1002/anie.202100870>.
146. Wu, W.; Fang, H.; Ma, H.; Wu, L.; Wang, Q.; Wang, H. Self-Powered Rewritable Electrochromic Display based on WO_{3-x} Film with Mechanochemically Synthesized MoO_{3-y} Nanosheets. *ACS Appl Mater Interfaces* **2021**, *13*, 20326–20335, <https://doi.org/10.1021/acsami.1c01959>.
147. Fu, X.; Lee, S.H.; Kuroiwa, Y.; Tatsuma, T. Near infrared electrochromic smart window with plasmonic compound nanomaterials. *Electrochemistry* **2021**, *89*, 141–144, <https://doi.org/10.5796/electrochemistry.20-00157>.
148. Khan, A.A.; Khan, M.Q.; Iqbal, M.; Abid, A.Y.; Khan, A.R.; Iqbal, Y.; Mahmood, R.; Khan, M.N. Facile synthesis of tungsten trioxide 3D architectures by a simple chemical solution route and photodegradation of Rhodamine B: structural, thermal, optical and impedance studies. *J Mater Sci Mater Electron* **2017**, *28*, 10357–10364, <https://doi.org/10.1007/s10854-017-6805-x>.
149. Deb, S.K. Optical and photoelectric properties and colour centres in thin films of tungsten oxide. *Philos Mag* **1973**, *27*, 801–822, <https://doi.org/10.1080/14786437308227562>.
150. Wang, Y.; Wang, S.; Wang, X.; Zhang, W.; Zheng, W.; Zhang, Y.M.; Zhang, S.X. A multicolour bistable electronic shelf label based on intramolecular proton-coupled electron transfer. *Nat Mater* **2019**, *18*, 1335–1342, <https://doi.org/10.1038/s41563-019-0471-8>.
151. Lang, A.W.; Österholm, A.M.; Reynolds, J.R. Paper-Based Electrochromic Devices Enabled by Nanocellulose-Coated Substrates. *Adv Funct Mater* **2019**, *29*, 1903487, <https://doi.org/10.1002/adfm.201903487>.
152. Cui, B.B.; Zhong, Y.W.; Yao, J. Three-state near-infrared electrochromism at the molecular scale. *J Am Chem Soc* **2015**, *137*, 4058–4061, <https://doi.org/10.1021/jacs.5b00586>.
153. Bao, X.; Zhao, Q.; Wang, H.; Liu, K.; Qiu, D. Metallopolymer electrochromic film prepared by oxidative electropolymerization of a Fe(II) complex with arylamine functionalized terpyridine ligand. *Inorg Chem Commun* **2013**, *38*, 88–91, <https://doi.org/10.1016/j.inoche.2013.10.008>.
154. Higuchi, M. Stimuli-responsive metallo-supramolecular polymer films: Design, synthesis and device fabrication. *J Mater Chem C* **2014**, *2*, 9331–9341, <https://doi.org/10.1039/c4tc00689e>.
155. Mondal, S.; Yoshida, T.; Rana, U.; Bera, M.K.; Higuchi, M. Thermally stable electrochromic devices using Fe(II)-based metallo-supramolecular polymer. *Sol Energy Mater Sol Cells* **2019**, *200*, 110000, <https://doi.org/10.1016/j.solmat.2019.110000>.
156. Mondal, S.; Ninomiya, Y.; Yoshida, T.; Mori, T.; Bera, M.K.; Ariga, K.; Higuchi, M. Dual-Branched Dense Hexagonal Fe (II)-Based Coordination Nanosheets with Red-to-Colorless Electrochromism and Durable Device Fabrication. *ACS Appl Mater Interfaces* **2020**, *12*, 31896–31903, <https://doi.org/10.1021/acsami.0c05921>.
157. Xing, J.; Yue, Y.; Zhang, R.; Liu, J. Molecular engineering of head-tail terpyridine-Fe(II) coordination polymers employing alkyl chain linkers toward enhanced electrochromic performance. *Dye Pigment* **2021**, *189*, 109233, <https://doi.org/10.1016/j.dyepig.2021.109233>.
158. Jittiarporn, P.; Badilescu, S.; Al Sawafta, M.N.; Sikong, L.; Truong, V. V. Electrochromic properties of sol-gel prepared hybrid transition metal oxides – A short review. *J Sci Adv Mater Devices* **2017**, *2*, 286–300, <https://doi.org/10.1016/j.jsamd.2017.08.005>.
159. Gies, M.; Michel, F.; Lupó, C.; Schlettwein, D.; Becker, M.; Polity, A. Electrochromic switching of tungsten oxide films grown by reactive ion-beam sputter deposition. *J Mater Sci* **2021**, *56*, 615–628, <https://doi.org/10.1007/s10853-020-05321-y>.
160. Liu, S.; Zhang, P.; Fu, J.; Wei, C.; Cai, G. A Mini-Review: Pyridyl-Based Coordination Polymers for Energy Efficient Electrochromic Application. *Front Energy Res* **2021**, *9*, 64, <https://doi.org/10.3389/fenrg.2021.620203>.
161. Dong, Y.; Luo, F.; Chen, L.; Yuan, F.; Hou, Y.; Li, W.; Yan, S.; Dai, Y.; Ouyang, M.; Zhang, C. Multi-color electrochromism containing green color based on electrochemically polymerized star-shaped phenyl bithiophene. *Phys Chem Chem Phys* **2018**, *20*, 12923–12928, <https://doi.org/10.1039/c8cp00338f>.
162. Sakamoto, R.; Tsukada, S.; Nishihara, H. Multinuclear metalladithiolenes: Focusing on electronic communication in mixed-valent states. *Dalt Trans* **2012**, *41*, 10123–10135, <https://doi.org/10.1039/c2dt30787a>.
163. Li, H.; Cao, J.; Zheng, W.; Chen, Y.; Wu, D.; Dang, W.; Wang, K.; Peng, H.; Liu, Z. Controlled synthesis of topological insulator nanoplate arrays on mica. *J Am Chem Soc* **2012**, *134*, 6132–6135,

- <https://doi.org/10.1021/ja3021395>.
164. Gehring, P.; Benia, H.M.; Weng, Y.; Dinnebier, R.; Ast, C.R.; Burghard, M.; Kern, K. A natural topological insulator. *Nano Lett* **2013**, *13*, 1179–1184, <https://doi.org/10.1021/nl304583m>.
165. König, M.; Wiedmann, S.; Brüne, C.; Roth, A.; Buhmann, H.; Molenkamp, L.W.; Qi, X.L.; Zhang, S.C. Quantum spin Hall insulator state in HgTe quantum wells. *Science* **2007**, *318*, 766–770, <https://doi.org/10.1126/science.1148047>.
166. Qi, X.L.; Zhang, S.C. Topological insulators and superconductors. *Rev Mod Phys* **2011**, *83*, 1057–1110, <https://doi.org/10.1103/RevModPhys.83.1057>.
167. Wang, Z.F.; Liu, Z.; Liu, F. Quantum anomalous hall effect in 2D organic topological insulators. *Phys Rev Lett* **2013**, *110*, 196801, <https://doi.org/10.1103/PhysRevLett.110.196801>.
168. Liu, Z.; Wang, Z.F.; Mei, J.W.; Wu, Y.S.; Liu, F. Flat chern band in a two-dimensional organometallic framework. *Phys Rev Lett* **2013**, *110*, 106804, <https://doi.org/10.1103/PhysRevLett.110.106804>.
169. Kato, R. Conducting metal dithiolene complexes: Structural and electronic properties. *Chem Rev* **2004**, *104*, 5319–5346, <https://doi.org/10.1021/cr030655t>.
170. Zheng, Z.; Nottbohm, C.T.; Turchanin, A.; Muzik, H.; Beyer, A.; Heilemann, M.; Sauer, M.; Götzhäuser, A. Janus-Nanomembranen: eine allgemein einsetzbare Basis für Chemie in zwei Dimensionen. *Angew Chemie* **2010**, *122*, 8671–8675, <https://doi.org/10.1002/ange.201004053>.
171. Kögel, J.F.; Kusaka, S.; Sakamoto, R.; Iwashima, T.; Tsuchiya, M.; Toyoda, R.; Matsuoka, R.; Tsukamoto, T.; Yuasa, J.; Kitagawa, Y.; Kawai, T. Heteroleptic [Bis(oxazoline)](dipyrrinato) zinc (II) complexes: bright and circularly polarized luminescence from an originally achiral dipyrrinato Ligand. *Angew Chemie - Int Ed* **2016**, *55*, 1377–1381, <https://doi.org/10.1002/anie.201509411>.
172. Tsuchiya, M.; Sakamoto, R.; Kusaka, S.; Kitagawa, Y.; Okumura, M.; Nishihara, H. Asymmetric dinuclear bis(dipyrrinato)zinc(ii) complexes: broad absorption and unidirectional quantitative exciton transmission. *Chem Commun* **2014**, *50*, 5881–5883, <https://doi.org/10.1039/c4cc01573h>.
173. Kusaka, S.; Sakamoto, R.; Kitagawa, Y.; Okumura, M.; Nishihara, H. An extremely bright heteroleptic bis(dipyrrinato)zinc(II) complex. *Chem - An Asian J* **2012**, *7*, 907–910, <https://doi.org/10.1002/asia.201200131>.
174. Kusaka, S.; Sakamoto, R.; Nishihara, H. Luminescent heteroleptic tris(dipyrrinato)indium(III) complexes. *Inorg Chem* **2014**, *53*, 3275–3277, <https://doi.org/10.1021/ic500326u>.
175. Baudron, S.A. Luminescent dipyrrin based metal complexes. *Dalt Trans* **2013**, *42*, 7498–7509, <https://doi.org/10.1039/c3dt50493j>.
176. Matsuoka, R.; Toyoda, R.; Sakamoto, R.; Tsuchiya, M.; Hoshiko, K.; Nagayama, T.; Nonoguchi, Y.; Sugimoto, K.; Nishibori, E.; Kawai, T.; Nishihara, H. Bis (dipyrrinato) metal (II) coordination polymers: crystallization, exfoliation into single wires, and electric conversion ability. *Chem Sci* **2015**, *6*, 2853–2858, <https://doi.org/10.1039/c5sc00273g>.
177. Sakamoto, R.; Iwashima, T.; Tsuchiya, M.; Toyoda, R.; Matsuoka, R.; Kögel, J.F.; Kusaka, S.; Hoshiko, K.; Yagi, T.; Nagayama, T.; Nishihara, H. New aspects in bis and tris (dipyrrinato) metal complexes: bright luminescence, self-assembled nanoarchitectures, and materials applications. *J Mater Chem A* **2015**, *3*, 15357–15371, <https://doi.org/10.1039/c5ta02040a>.
178. Sung, J.H.; Heo, H.; Si, S.; Kim, Y.H.; Noh, H.R.; Song, K.; Kim, J.; Lee, C.S.; Seo, S.Y.; Kim, D.H.; Kim, H.K. Coplanar semiconductor–metal circuitry defined on few-layer MoTe₂ via polymorphic heteroepitaxy. *Nat Nanotechnol* **2017**, *12*, 1064–1070, <https://doi.org/10.1038/nnano.2017.161>.
179. Holten, D.; Bocian, D.F.; Lindsey, J.S. Probing electronic communication in covalently linked multiporphyrin arrays. A guide to the rational design of molecular photonic devices. *Acc Chem Res* **2002**, *35*, 57–69, <https://doi.org/10.1021/ar970264z>.
180. Mustafar, S.; Wu, K.H.; Toyoda, R.; Takada, K.; Maeda, H.; Miyachi, M.; Sakamoto, R.; Nishihara, H. Electrochemical fabrication of one-dimensional porphyrinic wires on electrodes. *Inorg Chem Front* **2016**, *3*, 370–375, <https://doi.org/10.1039/c5qi00239g>.
181. Chung, I.; Lee, B.; He, J.; Chang, R.P.H.; Kanatzidis, M.G. All-solid-state dye-sensitized solar cells with high efficiency. *Nature* **2012**, *485*, 486–489, <https://doi.org/10.1038/nature11067>.
182. Yang, F.; Liu, J.; Lu, Z.; Dai, P.; Nakamura, T.; Wang, S.; Chen, L.; Wakamiya, A.; Matsuda, K. Recycled utilization of a nanoporous Au electrode for reduced fabrication cost of perovskite solar cells. *Adv Sci* **2020**, *7*, 1902474, <https://doi.org/10.1002/advs.201902474>.
183. Wang, Y.C.; Huang, S.K.; Nakamura, T.; Kao, Y.T.; Chiang, C.H.; Wang, D.Y.; Chang, Y.J.; Koshida, N.; Shimada, T.; Liu, S.; Chen, C.W. Quantum-assisted photoelectric gain effects in perovskite solar cells. *NPG Asia Mater* **2020**, *12*, 1–10, <https://doi.org/10.1038/s41427-020-00236-1>.
184. Liu, S.; Wang, Y.C.; Chang, C.M.; Yasuda, T.; Fukui, N.; Maeda, H.; Long, P.; Nakazato, K.; Jian, W.B.; Xie, W.; Tsukagoshi, K. Solution-processed organometallic quasi-two-dimensional nanosheets as a hole buffer layer for organic light-emitting devices. *Nanoscale* **2020**, *12*, 6983–6990, <https://doi.org/10.1039/d0nr00240b>.
185. Wang, Y.C.; Chiang, C.H.; Chang, C.M.; Maeda, H.; Fukui, N.; Wang, I.T.; Wen, C.Y.; Lu, K.C.; Huang, S.K.; Jian, W.B.; Chen, C.W.; Tsukagoshi, K.; Nishihara, H. Two-Dimensional Bis (dithiolene) iron (II) Self-Powered UV Photodetectors with Ultrahigh Air Stability. *Adv Sci* **2021**, *8*, 2100564,

- <https://doi.org/10.1002/advs.202100564>.
186. Arbulu, R.C.; Jiang, Y.B.; Peterson, E.J.; Qin, Y. Metal–Organic Framework (MOF) Nanorods, Nanotubes, and Nanowires. *Angew Chemie - Int Ed* **2018**, *57*, 5813–5817, <https://doi.org/10.1002/anie.201802694>.
187. Zhao, M.; Lu, Q.; Ma, Q.; Zhang, H. Two-Dimensional Metal–Organic Framework Nanosheets. *Small Methods* **2017**, *1*, 1600030, <https://doi.org/10.1002/smt.201600030>.
188. Ma, L.; Hou, B.; Shang, N.; Zhang, S.; Wang, C.; Zong, L.; Song, J.; Wang, J.; Zhao, X. The precise synthesis of twin-born Fe₃O₄/FeS/carbon nanosheets for high-rate lithium-ion batteries. *Mater Chem Front* **2021**, *5*, 4579–4588, <https://doi.org/10.1039/D1QM00153A>.
189. Koh, S.W.; Hu, J.; Hwang, J.; Yu, P.; Sun, Z.; Liu, Q.; Hong, W.; Ge, J.; Fei, J.; Han, B.; Liu, Z. Two-dimensional palladium diselenide for the oxygen reduction reaction. *Mater Chem Front* **2021**, *5*, 4970–4980, <https://doi.org/10.1039/D0QM01113D>.
190. Chang, Z.; Yang, D.H.; Xu, J.; Hu, T.L.; Bu, X.H. Flexible metal-organic frameworks: Recent advances and potential applications. *Adv Mater* **2015**, *27*, 5432–5441, <https://doi.org/10.1002/adma.201501523>.
191. Elsaidi, S.K.; Mohamed, M.H.; Banerjee, D.; Thallapally, P.K. Flexibility in Metal–Organic Frameworks: A fundamental understanding. *Coord Chem Rev* **2018**, *358*, 125–152, <https://doi.org/10.1016/j.ccr.2017.11.022>.